Geophysical Journal International

Geophys. J. Int. (2015) **201,** 621–639 doi: 10.1093/gji/ggv044
GJI Seismology

Field survey and modelling of the Caspian Sea tsunami of 1990 June 20

Amir Salaree and Emile A. Okal

Department of Earth and Planetary Sciences, Northwestern University, Evanston, IL 60208, *USA. E-mail: amir@earth.northwestern.edu*

Accepted 2015 January 21. Received 2015 January 20; in original form 2014 September 27

SUMMARY

The Rudbar-Tarom earthquake of 1990 June 20 ($M_0 = 1.4 \times 10^{27}$ dyn cm), the largest one in Iran over the past 35 yr, was accompanied by a small tsunami in the Caspian Sea, which produced run-ups of up to 2 m, and inundations of 1 km, reaffirming the existence of tsunami hazard along the Caspian shoreline, as suggested by historical reports. We present the results of a field survey, documenting the concentration of the effects of the tsunami along a section of coastline not exceeding 30 km in length. A hydrodynamic simulation using the earthquake dislocation as the source of the tsunami fails to reproduce both the amplitude of the waves, and especially their concentration between the cities of Kiashahr and Jafrood. Rather, we show that the model of an underwater landslide, presumably triggered by the earthquake, and taking place on the steep slopes of the continental shelf approximately 10 km offshore, can fit the principal inundation characteristics identified during the survey. We suggest that the occurrence of such underwater landslides should become a primary ingredient to the assessment of tsunami risk along the Southern shores of the Caspian Sea.

Key words: Tsunamis; Submarine landslides; Asia.

1 INTRODUCTION

Susceptibility to tsunamis is an important issue along the Iranian coastlines of the Caspian Sea due to their high population density. Among factors enhancing demographic hazard from potential tsunamis, we note the presence of major ports (e.g. Bandar-e-Turkaman and Bandar-e-Anzali), inadequate construction practices and the absence of highlands which could act as barriers or shelters against tsunami waves. In this context, some level of mitigation of their hazard can be expected from research into the occurrence of historical tsunamis and the identification of possible future sources of tsunamis in the region.

We are motivated in this respect by reports of tsunami occurrences on the southern shores of the Caspian Sea as found, among others, in Hedin (1892), Dotsenko *et al.* (2002), Zaitsev *et al.* (2004) and in Ambraseys & Melville's (1982) monumental compilation of the seismicity of Iran (Fig. 1).

Tsunami hazard in the southern Caspian Sea stems principally from the high level of seismicity of the Iranian plateau and in particular its northern region closest to the southern margins of the Sea (Fig. 2). In the general seismotectonic framework of the region (e.g. Mirzaei *et al.* 1999), seismic sources with the potential of generating tsunamis in the Caspian Sea include the Apsheron-Balkan belt at the northern boundary of the southern Caspian basin (e.g. Priestley *et al.* 1994; Jackson *et al.* 2002), the faulting systems in the northern Iranian plateau, extending to the southern coast of the Caspian Sea (e.g. Jackson *et al.* 2002; Aghanabati 2004), and the slopes on the western margin such as the Derbent basin (e.g. Polyakov *et al.* 2010), and northern margins of the Sea (e.g. Putans *et al.* 2010).

This seismicity is documented to have reached considerable hazard levels, with Ambraseys & Melville (1982) listing 36 events (most of them not tsunamigenic) of estimated $M > 6$, of which 11 have $M > 7$. In particular, the 22 December 856 $M \approx 7.9$ earthquake at Qumis (today's Semnan) and in the southeastern corner of the Sea resulted in about 250 000 casualties. The earthquake of 935 AD in Ray (about today's Tehran) was also a catastrophic event in north-central Persia (Ambraseys & Melville 1982). In modern times also, catastrophic earthquakes have occurred in the region, an example being the 1990 earthquake of Rudbar-Tarom ($M_S = 7.4$) which killed 13 000 people and injured 105 000, leaving a total of 7.2 billion USD economic loss (Berberian & Walker 2010). This event is the subject of our detailed study. We conclude that the 1990 tsunami was most likely due to a submarine landslide triggered by the earthquake.

1.1 Challenges and background events

Studying the history of tsunami occurrences in the Caspian Sea faces certain difficulties. First, considerable fluctuations in the Caspian Sea level (e.g. Rychagov 1997; Ozyavas & Khan 2012) on the order of several metres (Fig. 3) make the measurements of the evidence left by tsunamis extremely difficult if not practically impossible. This is mainly due to the fact that analyses of the deposits left by possible inundations (e.g. Cisternas *et al.* 2005) will be

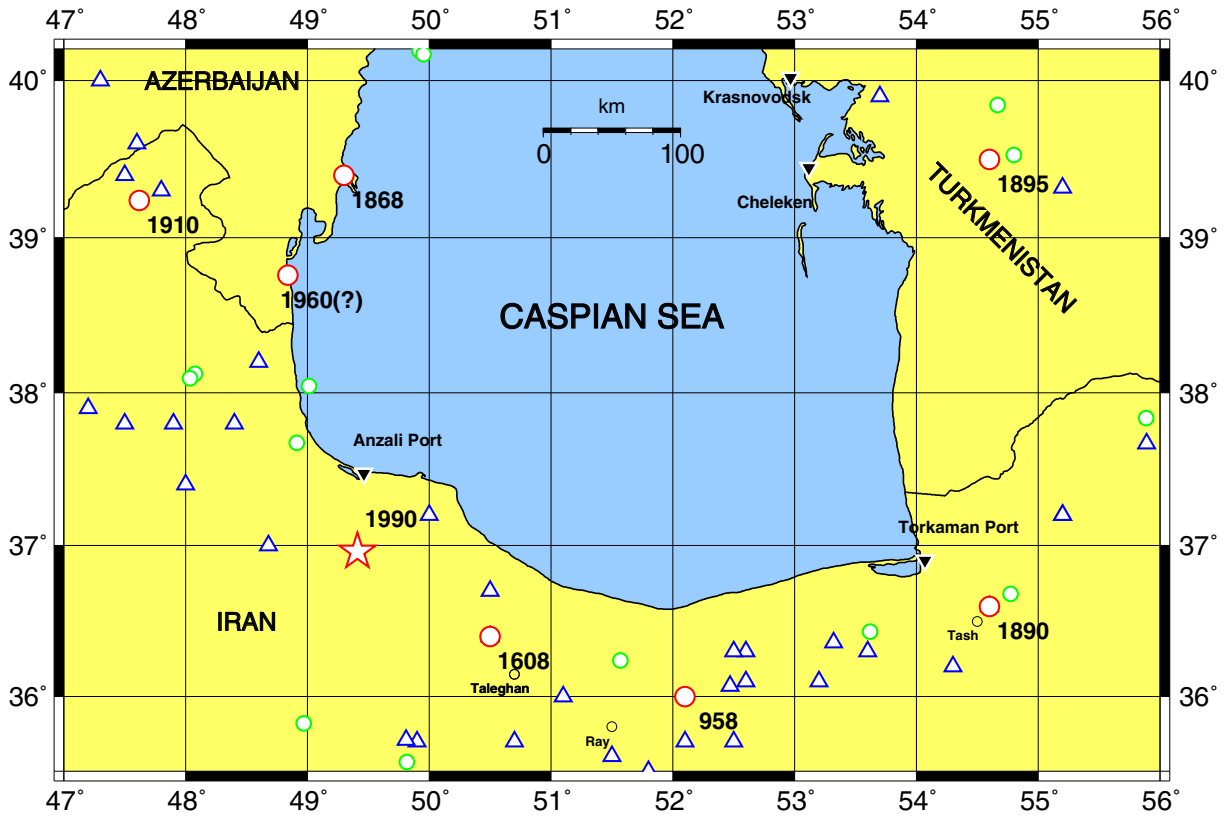

Figure 1. Historical tsunami sources surrounding the southern Caspian Sea (red circles) (Ambraseys & Melville 1982). Earthquake epicentres for $M_S > 6.0$ from the USGS catalogue (1900–2014) are shown with green circles. Epicentres for historical events reported by Ambraseys & Melville (1982) are depicted with blue triangles.

biased by numerous erratic long-term and short-term floodings over time (see Fig. 3). In addition, many such deposits could presently be below sea level.

Secondly, abrupt changes in the Caspian Sea level (e.g. Fig. 3; Ozyavas & Khan 2012) reduce the chance of tsunamis getting recorded in the memories of the inhabitants. As a result, looking for evidence of tsunami records in historical accounts is very difficult and thus scientific studies on modelling the past or possible future tsunamis in the Caspian Sea remain highly hypothetical and are not rigorously based on field data (e.g. Dotsenko *et al.* 2001, 2002; Soltanpour & Rastgoftar 2011).

Finally, the Iranian coastlines of the Caspian Sea have undergone substantial changes in the form of either cultivation or construction, especially over the past 40 yr. This adds another level of difficulty and complexity to the retrieving of the remaining information of the history of sea water surges.

In this general context, Ambraseys & Melville (1982) have identified six definitive or probable reports of tsunamis affecting the southern coast of the Caspian Sea in the past 1200 yr (Fig. 1), for only two of which, the 1608 Taleghan ($M \approx 7.6$) and 1890 Tash-Shahrood ($M \approx 7.2$) events, the source is well identified.

(i) It is suggested from several accounts of the 23 February 958 earthquake of Ray (e.g. Gerasimov 1978) that possibly the event was connected with abnormal changes in the Caspian Sea level, but the evidence is not conclusive and the historical references might have originally been to the Persian Gulf.

(ii) The accounts of the 1608 April 20 earthquake of Taleghan, however, are much more reliable. As a result of this event, large waves were generated in the Caspian Sea creating great alarm (Ambraseys & Melville 1982).

(iii) Hedin (1892) reports that the sea waves from the 1890 July 11 event in Tash-Shahrood (Fig. 1) had reached as far as the Anzali port, about 400 km to the west, but there is no other quantitative description about the nature of the excited waves.

(iv) Reports of the earthquake of 1895 July 8 in Krasnovodsk (Turkmenistan) include accounts of water surges inundating the coastal area. Kondorskaya *et al.* (1982) (who assign $M_S \approx 8.2$ to the event) report that an entire part of the island of Uzun-Ada was rapidly covered by water and go on to say '... huge waves gushed from the sea and flooded the buildings and docks ... There was a terrifying roar during the powerful shaking. The water in the harbour quickly swelled high and reached the railroad tracks.' Ambraseys (1997), who corrected the magnitude to $M_S = 7.2$ using the Prague formula, reports seawaves flooding the coast of Cheleken Island. He also mentions extensive bathymetry changes in the region off the coast of Krasnovodsk, perhaps due to submarine landslides.

(v) Ambraseys & Melville (1982) mention reports of large sea waves in the Caspian Sea as a result of events on 1868 April 26 and 1910 December 4 at Baku and Mughan, but unfortunately no earthquakes capable of creating such waves have been recorded or documented.

(vi) Rikhter (1961) mentions an abnormal subsidence of the sea level at Baku and other south Caspian sites on 1960 April 26, by as much as 1 m over 2 or 3 hr, followed by a sharp rise, a new drop and then another rise which he attributes to an earthquake in Iran which had occurred two days before. However, as detailed in the Appendix, the interpretation of this report as a tsunami originating

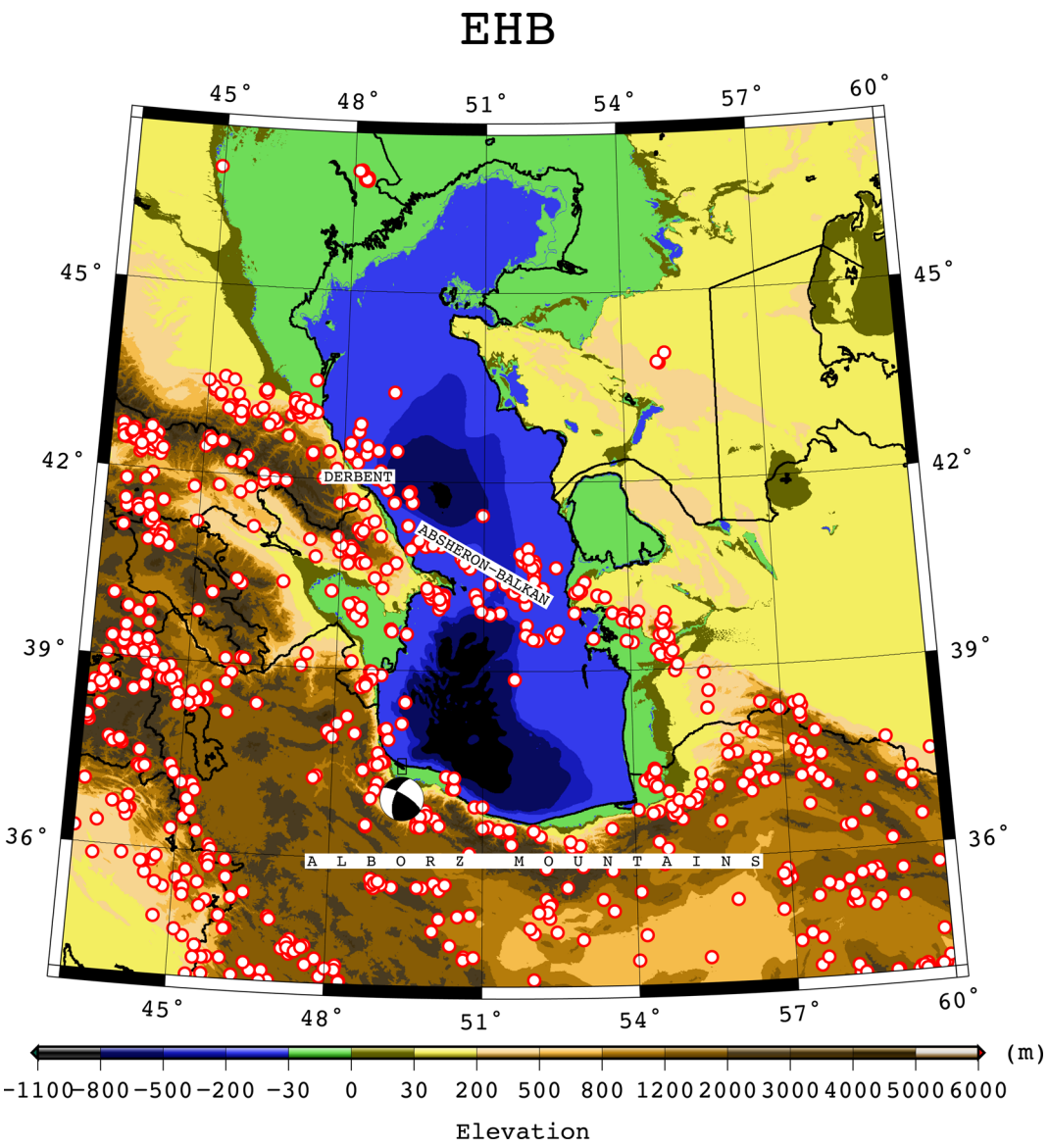

Figure 2. Seismicity of the northern Iranian plateau and the Caspian Sea region. Red circles are epicentres of earthquakes (1900–2014) from the EHB catalogue. The focal mechanism is the CMT solution for the 20 June, 1990 Rudbar earthquake.

from a geological event can be discounted in view of its purported characteristics.

2 2012 FIELDWORK

Considering the few studies mentioned above, our knowledge about the history of tsunami occurrences in the Caspian Sea and the events causing them is merely based on historical records and no quantitative scientific evidence has been reported. As a result, a field survey was conducted along the southern Caspian Sea (i.e. Iranian) coastlines. Its main goal was initially to look for historical evidence in the region, and in particular, to seek any additional possible evidence for the 1960 event reported by Rikhter (1961). While this event remains largely putative, it seemed that it might be the only one recent enough to be still remembered by the older population of the region, possibly lending itself to a field survey using conventional methods based on human recollection, as described by Synolakis *et al.* (2002).

The survey along the southern coastlines of the Caspian Sea was conducted between 2012 August 21 and 2012 August 26. The original plan was to cover the entire Iranian coastal area of the Caspian Sea, but according to the recent drastic water level changes of the Sea which has caused it to recede by a few kilometres in the easternmost section of the coastline (areas probably most affected by the 1890 event; Fig. 1) as well as other logistical issues, the eastern segments were not covered during the survey. The survey started from the Noshahr port area proceeding to Naftchal in the east and then back from Noshahr to Astara in the west (Fig. 4 and Table 1).

As can be seen from Table 1, the majority of the elderly witnesses we interviewed did not remember any tsunami events. By contrast, six witnesses shared distinctive memories of inundation following the Rudbar earthquake of 1990 June 20. These testimonies constituted an unexpected development since to our best knowledge, this tsunami had not been previously reported in the literature. On the other hand, the 1990 earthquake was clearly the largest event recorded in northern Iran during the era of instrumental

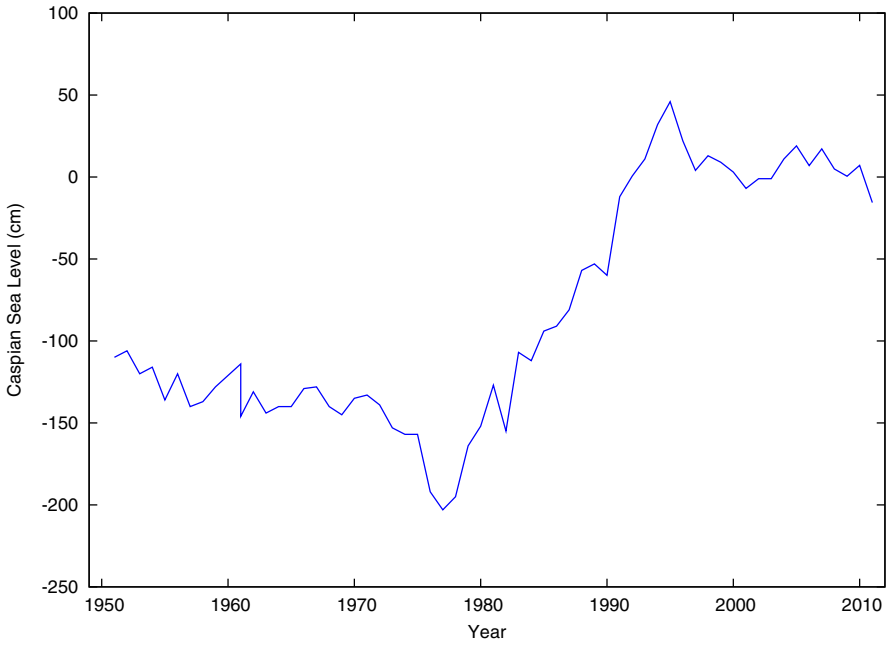

Figure 3. Caspian sea level changes over the past 60 yr. The 'zero' level refers to 26.1562 m below the standard ocean surface (Port Captain, Noshahr, Iran, personal communication, 2012).

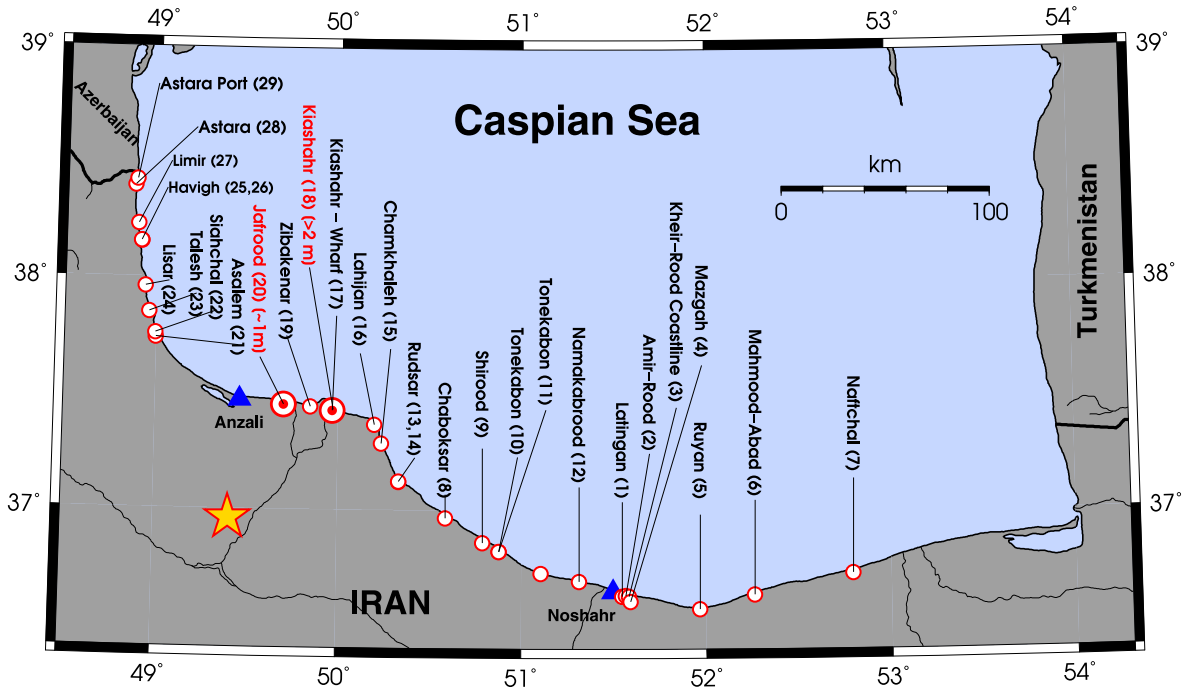

Figure 4. Geographical distribution of the interview points in this study. Anzali and Noshahr ports are depicted by blue triangles. The yellow star denotes the epicentre of the 1990 Rudbar earthquake. Numbers in this figure are location numbers from Table 1. The two bull's-eyes represent the major run-up reports from the survey.

seismology and thus constitutes the best candidate to generate a local tsunami.

2.1 1990 June 20 tsunami

During the survey, it was discovered that the Rudbar-Tarom earthquake (see Section 3) had caused a tsunami in the southern Caspian Sea as two grade *a* and one grade *b* observations at Kiashahr, Jafrood and Chaboksar (numbers 17, 20 and 8 in Table 1, respectively) revealed sea water surges after the earthquake. Although this total number of observations is low, these testimonies were too detailed to be ignored, and thus constitute a reliable basis for the study of the 1990 tsunami.

2.1.1 Chaboksar

Chaboksar is a tourist town in the Gilan province of Iran and is among the closest towns to the Caspian Sea. Safar Fallah, a former

Table 1. Data summary from the 2012 fieldwork on the Southern Caspian Sea shorelines. The *quality* column represents the reliablity and accuracy of the accounts in an *a* to *d* scale with *a* and *d* as the most and least reliable respectively. 'IN', 'RU', 'NOW' and 'EY' stand for *inundation*, *run-up*, *number of waves* and *event year*.

No.	Longitude	Latitude	IN (m)	RU (m)	NOW	EY	Quality	Location
1	51.54613	36.62939	NA	NA	NA	NA	NA	Latingan
2	51.56684	36.63335	NA	NA	NA	NA	NA	Amir-Rood
3	51.58219	36.62886	NA	NA	NA	NA	NA	Kheir-Rood
4	51.59166	36.60733	NA	NA	NA	NA	NA	Mazgah
5	51.96721	36.57378	NA	NA	NA	NA	NA	Ruyan
6	52.26101	36.63633	NA	NA	NA	NA	NA	Mahmood-Abad
7	52.79466	36.72776	NA	NA	NA	NA	NA	Naftchal
8	50.58892	36.96689	NA	1	1	1990	b	Chaboksar
9	50.79047	36.86068	9	NA	4	∼1960	c	Shirood
10	50.87952	36.82203	NA	NA	NA	NA	NA	Tonekabon
11	50.87966	36.82217	NA	NA	NA	NA	NA	Tonekabon
12	51.3135	36.69367	10	1	NA	1990	d	Namakabrood
13	50.33305	37.12354	500	NA	NA	1990	d	Rudsar
14	50.33326	37.12406	NA	NA	NA	NA	NA	Rudsar
15	50.23764	37.28812	NA	NA	NA	NA	NA	Chamkhaleh
16	50.19915	37.37032	20	NA	NA	NA	NA	Lahijan
17	49.96856	37.42988	1000	>2	3	1990	a	Kiashahr
18	49.97272	37.43399	NA	NA	NA	NA	NA	Kiashahr
19	49.84914	37.44544	NA	NA	NA	2007?	b	Zibakenar
20	49.70346	37.45382	40	∼1-2	NA	1990	a	Jafrood
21	48.99825	37.73876	NA	NA	NA	NA	NA	Asalem
22	48.99557	37.75734	200	1	5	∼1960	a	Siahchal
23	48.96038	37.84928	∼100	NA	3	∼1970?	c	Talesh
24	48.93615	37.95877	NA	NA	NA	NA	NA	Lisar
25	48.91313	38.1537	NA	NA	NA	1990	d	Havigh
26	48.91069	38.1561	NA	NA	NA	NA	NA	Havigh
27	48.89332	38.22969	NA	NA	NA	∼1960	d	Limir
28	48.87225	38.39572	NA	NA	NA	NA	NA	Astara
29	48.88037	38.42246	NA	NA	NA	NA	NA	Astara Port

fisherman, recalled hearing from his then fellow fishermen who had been working in the sea far from Chaboksar (probably to the west) that after the 1990 earthquake, at midnight (see Section 3) there was one wave ∼1 m high reaching their fishing boats.

He also told the survey that around 20–30 yr ago, that is at the time of the Rudbar earthquake, the shoreline used to be some 500 m further in the sea with respect to its present position.

2.1.2 Kiashahr—the wooden wharf

Kiashahr is a low-altitude coastal town with a flat sand shoreline. The Kiashahr port is located on the eastern side of a delta formed by the Sefidrood river into the Caspian Sea. It has a lagoon with a wooden wharf which makes fishing possible and easy. However, it has gradually switched to a base for tourist boats. The ferrymen, former fishermen, at the wharf remember the Rudbar earthquake vividly as it was strongly felt in this area.

According to Seyed Yahya Hosseini, a former fisherman, the sea water had inundated the land to about 1000 m (with respect to the position of the shoreline at the time) and a run-up of more than 2 m had occurred. He recalled that there were three waves almost 2 hr after the main shock. The water had remained for about 5–10 min on the shore and then had receded to the sea, leaving dead fish on the coastal area. The 3–4 m long weeds were bent to south–southeast as a result of the waves. This reported delay is a critical datum, since it suggests that the tsunami was generated by a phenomenon ancillary to the earthquake and probably triggered by it, rather than directly by the dislocation itself.

Seyed Yahya's fellow fishermen who had been working on their boats at sea had reported waves a few metres high in the sea. They had also heard a rumble after the earthquake.

2.1.3 Jafrood

Jafrood is a low-altitude fishing village by the Caspian Sea in the Gilan province with population composed mostly of fishermen. According to Behzad, a fisherman, a 30–40 m inundation had occurred after the earthquake, making run-ups as high as 1 m. The sea water had then left the beach, going back up to about 3 m behind its former position.

2.1.4 Other locations

No reliable recollection of a tsunami event was found at the rest of the locations visited during the survey. Some witnesses gave us vague reports of events in the past, but such reports were unreliable and could not be confirmed. Thus, the evidence from the 1990 tsunami was only found at a narrow stretch of shoreline (∼30–40 km) from Kiashahr to Jafrood.

In this context, the lack of recollection of any tsunami inundation by reliable witnesses who recall vividly the shaking produced by the 1990 earthquake, can be interpreted as a datum, which in turn will constrain the distribution of flooding along the coastline. This takes the form of a probable maximum height of the waves. The latter which remains somewhat subjective, will depend on the topography of the shoreline. In the easternmost part of our field survey, east of

52.26°E (Naftchal), where the beach is extremely flat, we estimate a run-up threshold of 0.25 m, given that any larger wave would have penetrated several hundred meters inland. Taking into account the change in shoreline topography, this threshold is progressively increased, to 0.5 m west of 49.74°E, 1 m west of 49.22°E, and finally 2 m west of 48.9°E, where the coast features significant beach ridges. The resulting distribution of maximum wave heights outside the area of the reported tsunami will be used in our modelling efforts as a further constraint in Section 4.

In conclusion, this survey, originally meant to document the observation reported by Rikhter (1961), established that the major 1990 Rudbar earthquake was definitely accompanied by a local tsunami in the Caspian Sea. Its major features are a run-up reaching >2 m, but concentrated on a relatively narrow section of the coastline, extending no more than ∼40 km from Jafrood to Kiashahr, and a delay of about 2 hr with respect to the shaking during the earthquake. These features, and especially the limited lateral extent of the inundation, will constitute the observables to be matched by our simulation effort in Section 4. In addition, metre-size waves were reported by fishermen at sea.

3 THE RUDBAR-TAROM EARTHQUAKE

The Rudbar-Tarom (most commonly known as Rudbar) earthquake, $M_w = 7.4$, occurred on 1990 June 20 at 21:00:13 UTC (00:30:13 on June 21, local time) and was one of the most destructive recorded seismic events in Iran (Berberian *et al.* 1992). In addition to the standard Harvard CMT and NEIC solutions, several studies such as Berberian *et al.* (1992), Ishihara *et al.* (1992), Campos *et al.* (1994), Virieux *et al.* (1994), Gao & Wallace (1995), Tatar & Hatzfeld (2009) and Berberian & Walker (2010), have addressed its source mechanism (see Table 2). All of these mechanisms involve a generally steep-dipping fault plane striking 290°–315° (i.e. oriented along the general trend of the Alborz mountain range), along which a significant left-lateral strike-slip motion took place.

As detailed by Berberian & Walker (2010), the emerging picture is that of a 'surprising' strike-slip earthquake occurring in the generally compressional environment of the Alborz orogeny. As such, the 1990 Rudbar earthquake expresses partitioning of the oblique motion between central Iran and the Caspian Sea block, as defined by GPS investigations (Vernant *et al.* 2004). Beyond that overall left-lateral character, there remains a lack of consensus in the literature about the geometry of the host fault system (e.g. Berberian & Walker 2010).

Based on seismic analyses and geological evidence, Berberian & Walker (2010) propose that the earthquake was associated with 80 km of NW–SE trending left-lateral strike-slip faulting with an unusually large vertical displacement in the opposite sense of the existing topography (see Table 1). This model is upheld both by the distribution of aftershocks (Fig. 5) and by the composite rupture study of Campos *et al.* (1994) and Virieux *et al.* (1994), who model the 1990 earthquake as composed of nine subevents with a total duration of 25 s, based on the inversion of body and surface waves (Table 3). The rupture is then believed to have occurred bilaterally with a longer propagation to the southeast (Campos *et al.* 1994; Berberian & Walker 2010) (see Table 3).

In this context, we will use Mansinha & Smylie's (1971) algorithm to express the static displacement resulting from the Rudbar earthquake, which will be used as an initial condition in tsunami simulations. We will consider both a single source whose parameters are derived using scaling laws (Geller 1976) and the composite source of Campos *et al.* (1994), made up of nine individual subevents (see Table 3).

4 TSUNAMI: NUMERICAL MODELLING

4.1 Method

We simulated the 1990 June 20 tsunami by means of the MOST—Method Of Splitting Tsunami—algorithm (Titov & Synolakis 1995; Titov & González 1997; Titov & Synolakis 1998), which uses the fractional steps method originally developed by Yanenko (1971) to reduce the 2 + 1 problem of solving the 2-D differential shallow water version of Navier-Stokes equations into two simultaneous 1 + 1 problems. MOST is widely implemented in the modelling and study of tsunamis in various basins (e.g. Titov & González 1997). It has been validated rigorously by benchmarking against laboratory experiments. All relevant details can be found in Synolakis *et al.* (2008). In the present simulation, we verified *a posteriori* the appropriateness of the shallow water approximation ($f \ll \sqrt{g/h}$) given dominant frequencies on the order of ≈3 mHz and depths h of at most 1000 m.

In the present context and given the significant variations in the coastline over the past 25 yr, we do not compute run-up on initially

Table 2. Source parameters for the 1990 Rudbar earthquake from various studies (modified from Berberian & Walker 2010). M_0, ϕ, δ, λ, H and K.A. stand for *seismic moment*, *strike*, *dip*, *rake*, *depth* and *Kagan angle* [which expresses the solid rotation between a mechanism and the Harvard CMT, as defined by Kagan (1991)].

Study	M_0 ($\times 10^{27}$ dyn cm)	ϕ (°)	δ (°)	λ (°)	H (km)	K.A. (°)
HRVD[a]	1.4	300	73	32	15[b]	–
NEIC[c]	1.1	311	76	54	17	23
NEIC[d]	2.0	288	88	–11	19	44
Gao & Wallace (1995)[e]	1.4	288	88	–9	13	43
Berberian *et al.* (1992)[f]	0.88	292	88	–9	14	43
Campos *et al.* (1994)[f]	1.2	300	75	15	5–10	17
Campos *et al.* (1994)[e]	1.05	301	81.6	4.8	11.7	29

[a]CMT.
[b]Fixed depth.
[c]Best double-couple.
[d] *P*-waves fault plane solution.
[e]Body waves.
[f]Surface waves.

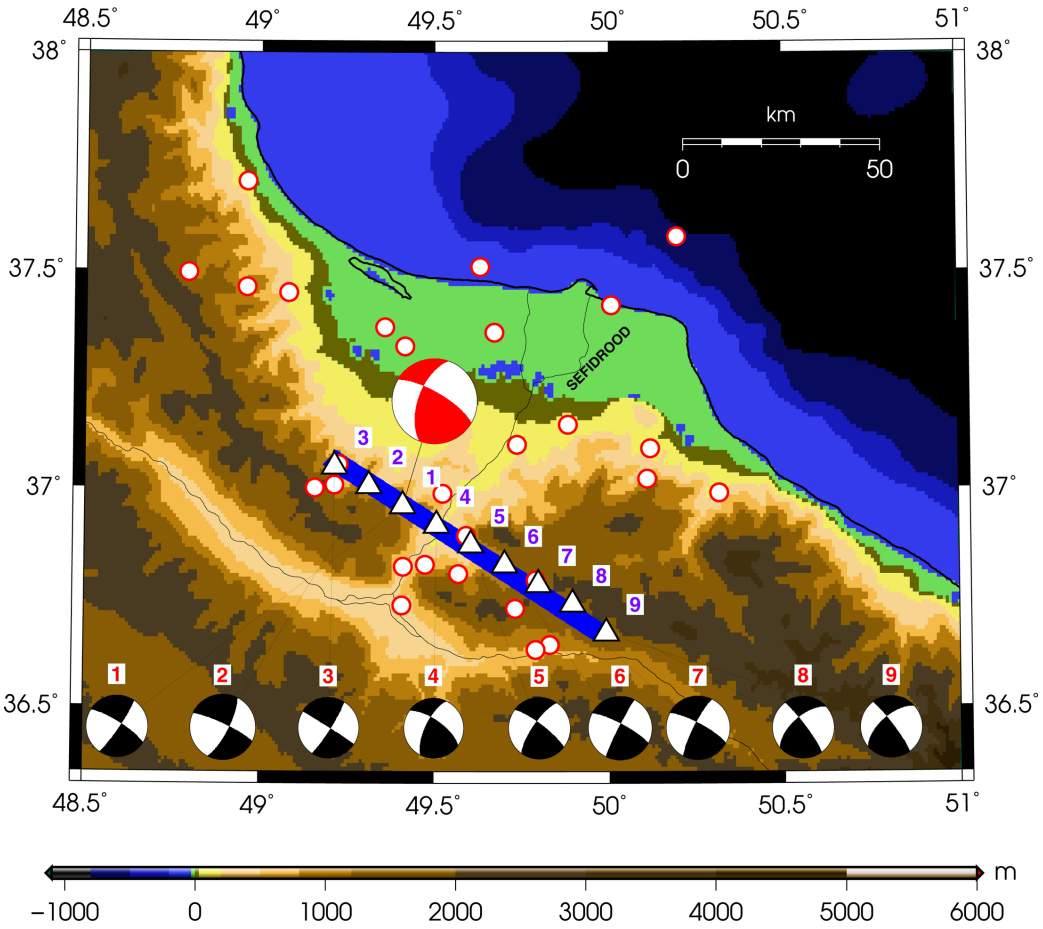

Figure 5. Map of the 1990 Rudbar earthquake with CMT mechanism (red beachball) and its aftershocks during the first 24 hr (red circles; from USGS). Also shown are the nine subevents (triangles) of Campos *et al.*'s (1994) model with respective focal mechanisms (indices referring to Table 3). The dark blue bar represents the length of faulting as used in the single event dislocation model.

Table 3. Subevents attributes for the 1990 Rudbar earthquake (Campos *et al.* 1994). M_0, ϕ, δ, λ, H, D, AZ and T stand for *seismic moment*, *strike*, *dip*, *rake*, *depth*, *distance to nucleation point*, *rupture azimuth* and *Time from start (lag)*, respectively.

Subevent	M_0 ($\times 10^{27}$ dyn cm)	ϕ (°)	δ (°)	λ (°)	H (km)	D	AZ (°)	T (s)
1	0.167	302.5	78.4	–6.9	11.1	0	0	0
2	0.62	295.1	81.4	–15.3	11.6	10	300	4
3	0.114	302.3	88.3	–7.2	14.4	20	300	8
4	0.069	304.9	68.3	24.6	9.9	10	120	4
5	0.131	307.8	79.4	16.7	12.5	20	120	10
6	0.275	298.3	79.1	4.3	10.7	30	120	12
7	0.263	298.6	78.8	9.7	5.6	40	120	16
8	0.130	323.3	83.6	28.7	4.4	50	120	20
9	0.044	330.5	98.6	46.1	10.9	60	120	24

dry land, but rather stop the computation at a depth of 3 m. While not allowing direct modelling of absolute run-up, this strategy can nevertheless model the relative amplitudes of the tsunami along the beach in the absence of short embayments and promontories.

4.2 Bathymetry data

Tsunami simulations require an adequate grid of bathymetric data. In our study and due to the lack of appropriate local bathymetry maps for the Caspian Sea, we had to use global bathymetry grids. We used the GEBCO bathymetric data set (Fisher *et al.* 1982) with a resolution of 30 arcsec (926 m in latitude). For the Caspian Sea region, it was compiled from over 280 000 bathymetric soundings and points digitized from bathymetric contours, taken from 107 Russian hydrographic charts which were constructed at a spacing of 0.1 min and then degraded to 30 s for inclusion in the GEBCO global data set. Our grid consists of 1200 longitude samples and 1700 latitude samples, corresponding to an average mesh size of ~750 m in longitude.

The choice of GEBCO over other potential sources of bathymetry (e.g. ETOPO1, Amante & Eakins 2009) was motivated by its higher resolution (30 arcsec) and the fact that it was compiled from more detailed sources. Finally, the GEBCO bathymetry model for the Caspian Sea agrees better with documented slumps in the western

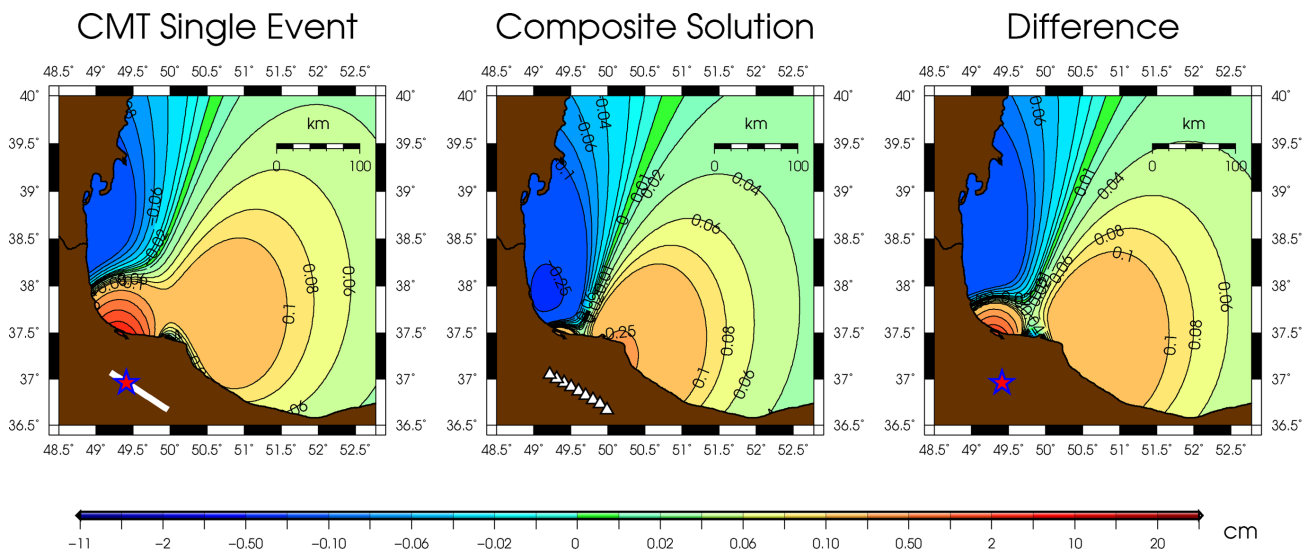

Figure 6. Vertical surface displacement fields for the 1990 Rudbar earthquake (in centimetres) for a single source, a composite source, and the difference between the two, as calculated using Mansinha & Smylie's (1971) algorithm. The red star, the triangles and the white bar represent the CMT epicentre of the main shock, the subevents' locations and the fault-line inferred from the aftershocks. The amplitudes at sea are on the order of at most a few centimetres.

margin of the Sea (Verzhbitskii *et al.* 2009a,b; Polyakov *et al.* 2010; Putans *et al.* 2010).

4.3 Simulation: earthquake source

As the initial condition to the equations of hydrodynamics, and in the case of earthquake sources, MOST uses the field of static deformations of the epicentral area resulting from the dislocation, as computed for example through the algorithms of Chinnery (1961), Mansinha & Smylie (1971) or Okada (1985).

By considering static deformations, we do not include the temporal evolution of the source, and as such use the centroid of the earthquake as its source. However, one can describe complex events as a superposition of individual subevents, each of them modelled in this fashion. In this study, we use both a single event modelled after the Harvard CMT solution, and the suite of subevents described by Campos *et al.* (1994).

In order to use the above algorithms, either for a single source or a combination of subevents, one needs to know the full geometry of the dislocation vector on the fault plane. Since such information is not accurately accessible especially in the case of subevents [as mentioned before, there is no consensus in the literature, e.g. Berberian & Walker (2010)], we have used the scaling laws developed by Geller (1976), which approximate the fault dimensions as $L \approx 2W$, where L and W are length and width of the fault plane respectively, and further assume a constant stress drop. As discussed, for example by Scholz (1982), such assumptions may break down for events with large magnitudes for which fault width (or slip or both) may be limited at the brittle–ductile transition, but should remain valid at the moment level of the Rudbar event (1.4×10^{27} dyn cm or $M_w = 7.4$). For the single source, Geller's (1976) scaling laws lead to $L = 65$ km, $W = 32$ km and $\Delta u = 1.9$ m. Note that this length agrees well with the distribution of the first day aftershocks (Fig. 5).

In this study, we used Mansinha & Smylie's (1971) formalism, the surface ground displacement being calculated both for the single-event and multiple-subevents cases. As shown on Fig. 6, the vertical displacements in the Caspian Sea are on the order of only a few millimetres for the individual subevents and a few centimetres in the case of the single shock or composite solution. However, Fig. 6 shows that the resulting fields differ slightly (by up to a few millimetres) for the single and composite sources. This expresses the fact that the composite source features more seismic release at the southeast end of the rupture (which is farther away from the coastline) in the models of Berberian & Walker (2010) and Campos *et al.* (1994).

The centimetric values of the initial deformation at sea reflect the concentration of most of the static field on land and suggest that the amplitude of the resulted tsunami should remain modest.

Our computations use a time step $\delta t = 3$ s (which satisfies the Courant–Friedrichs–Lewy condition for stability) and are performed for a total duration of 6 hr. The products of our simulations are twofold: we present in Fig. 7 the maximum positive amplitude reached during the simulation at each point of the grid, and also retain full time-series at 128 virtual gauges. The latter are positioned in the vicinity of our survey, extending ∼140 km along the coastline.

In the case of the composite source, we elected to run tsunami simulations for each of the individual sources, and to then sum the resulting wavefields allowing for time lags at the source. This allows us to explore the potential influence of the dynamic nature of the source, that is of the time lags separating the individual sources in the model of Campos *et al.* (1994).

This approach, which uses a linear combination of simulations from the individual subevents, is made possible by the low ratio of the maximum initial amplitudes to the depth of the water column, which makes the non-linear effect of amplitude dispersion negligible, that is the velocity of the tsunami under the shallow-water approximation which should be $c(x, y, t) = \sqrt{g.[h(x, y) + \eta(x, y, t)]}$ where $h(x, y)$ is the thickness of the unperturbed water column and η the vertical deformation of the surface, can be approximated as $c(x, y) = \sqrt{g.h(x, y)}$.

In addition, Figs 8 and 9 show that the difference between the static and dynamic simulations (i.e. neglecting or including the time lags between individual subevents) remains negligible. This is readily expected by the small ratio of those lags (≤25 s; see Table 3) to the typical periods of the simulated tsunami time-series (∼2500 s).

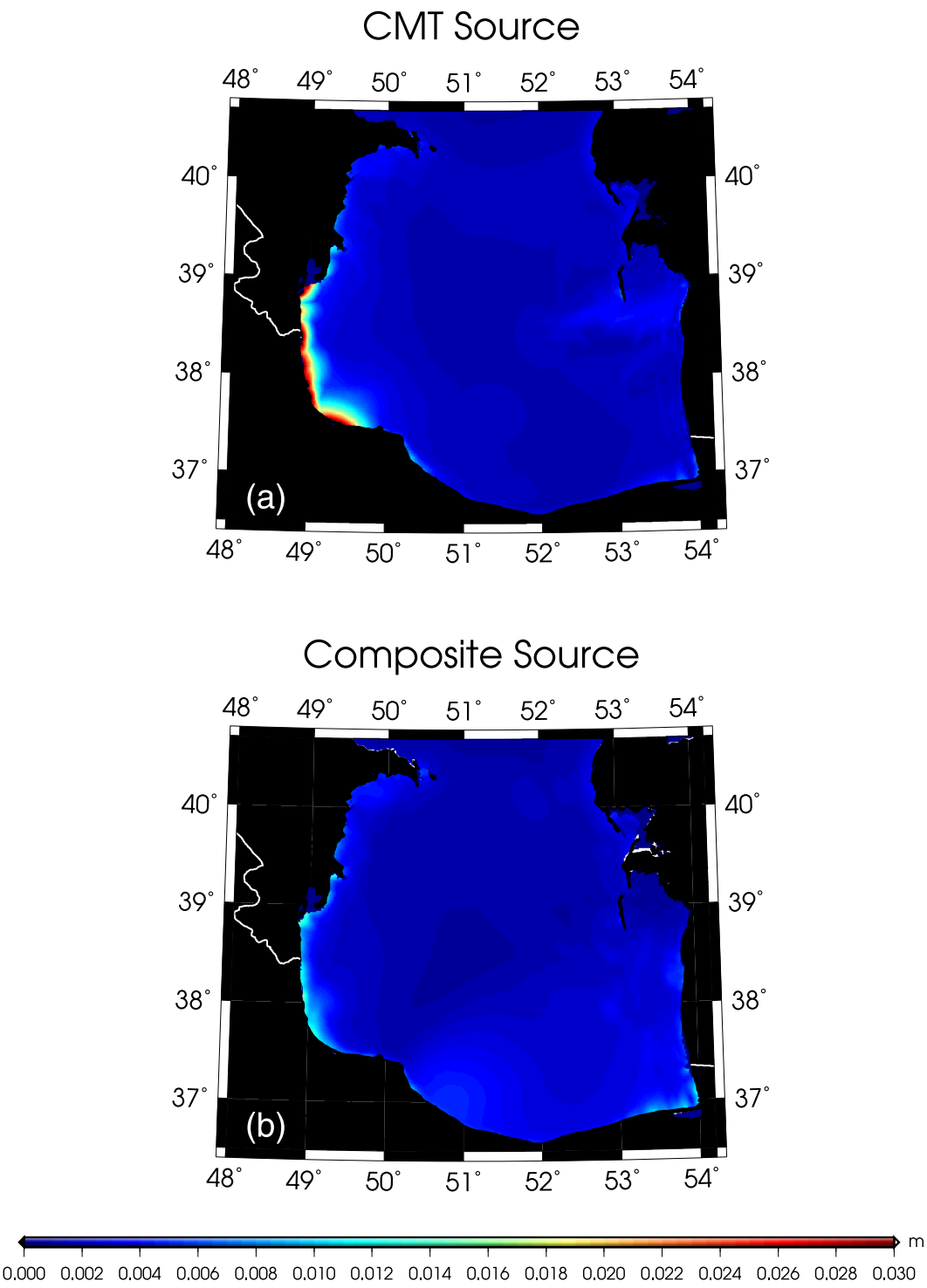

Figure 7. Distribution of maximum amplitudes in the southern Caspian for the CMT single source (a) and the composite source of nine subevents (b).

Results from the various simulations with earthquake sources are given on Figs 7–9. While they expectedly feature minor differences, all these models predict a maximum of inundation in the northwesternmost part of the study area, that is west of Kiashahr and in particular, they fail to reproduce the concentration of maximum amplitudes documented by our survey around the Anzali promontory.

In addition, we note that the maximum amplitudes simulated at the 3-m gauges do not exceed 1 cm. Notwithstanding the difficulty of predicting run-up on the coastline from amplitudes at the virtual gauges, we note that the amplification necessary to account for the observed values of ∼2 m documented by the survey should be on the order of a factor of 200, which appears excessive in the absence of significant embayments along that section of coastline (e.g. Reymond *et al.* 2012).

Finally, the simulated amplitudes at sea, which remain at most centimetric, cannot be reconciled with the accounts of waves reaching 1 m or more obtained during our field survey from the

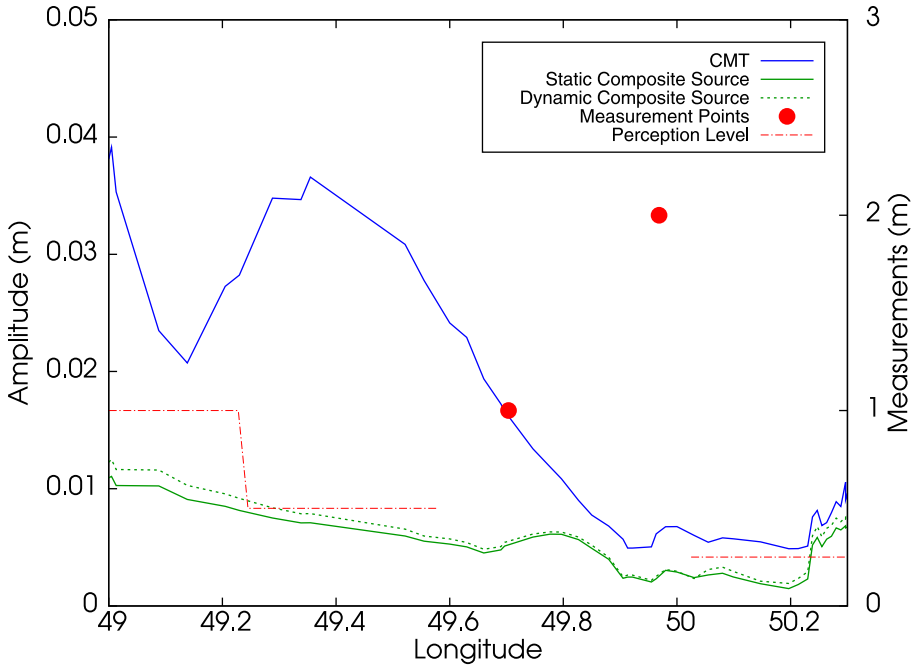

Figure 8. Tsunami amplitude distribution along the southwestern portion of the Caspian Sea coastline for different scenarios for the earthquake source (left-hand vertical axis) compared with the reported values from our survey (right-hand vertical axis). The difference between the amplitudes caused by the static and dynamic composite sources is negligible. Computed amplitudes for the CMT single source are within the same order of magnitude. The vertical axes are on different scales and clearly, the earthquake model fails to replicate the distribution of the observed data.

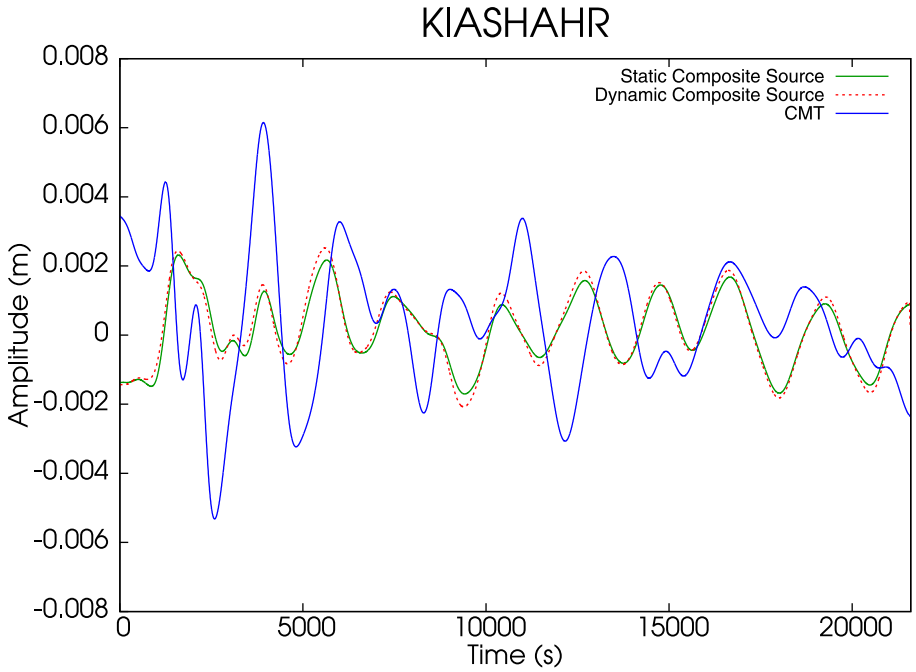

Figure 9. Comparison of the static and dynamic composite sources with the Harvard single event computed at Kiashahr.

reports of fishermen fishing in deep water the night of the earthquake. It is clear from our simulation that the tsunami generated by the seismic dislocation could not have been noticed on the high seas.

In conclusion, neither of the various earthquake dislocation sources considered here can adequately model the surveyed data set, most importantly its concentration around a 30-km stretch of coastline from Kiashahr to Jafrood.

4.4 Simulation: landslide source

The fact that the earthquake source model for the 1990 tsunami is unable to explain the field observations, along with the delay time of the wave arrivals with respect to the main shock reported at Kiashahr and the rumble heard by fishermen at sea at about the time of the surges, all suggest that the tsunami may have occurred as a result of a submarine landslide, presumably triggered by the earthquake.

The possibility that landslides triggered by earthquakes can be principal or exclusive contributors to catastrophic tsunamis was first expressed more than 100 yr ago by Verbeek (1900) and Montessus de Ballore (1907) and later revived by Imamura & Kennedy (1937) and Gutenberg (1939) who emphasized that the concept could explain the generation of a tsunami by an earthquake whose source is largely contained on land, classical examples being events of 1899 in Ceram (Verbeek 1900), 1910 at Rukwa (Ambraseys 1991), possibly 1922 in Chile (Gutenberg 1939) and more recently 2013 in Pakistan (Hoffmann *et al.* 2014).

Landslide tsunamis have been the subject of many studies and are understood reasonably well on both theoretical and experimental grounds, despite the inherently hidden character of their source. Skempton (1953) and Locat & Lee (2002) describe how landslides geologically evolve on the sea slopes. Synolakis *et al.* (2002) and Okal & Synolakis (2004) model them as hydrodynamic dipoles which are formed as negative (trough) and positive (hump) initial displacements caused by a rigid body of sediments and rocks moving from the former to the latter. This assumption, although simplistic [since submarine landslides will actually deform during their course as studied and modelled e.g. by Weiss *et al.* (2013) and Ma *et al.* (2013)], is successful in predicting the run-up values observed on real coastlines, at least at first order (e.g. Synolakis *et al.* 2002; Okal *et al.* 2009). Previous studies such as Hammack's (1973) and Heinrich's (1992) have successfully applied the rigid slump model to laboratory and computational experiments.

In this study, we used the method initially developed by Synolakis *et al.* (2002) to investigate a possible landslide scenario for the 1990 tsunami in the Caspian Sea. In this formalism, hump and trough are modelled as hyperbolic functions smoothed by a Gaussian function. The dipole is assumed to exist at $t = 0^+$, meaning that both the trough and the hump exist simultaneously and thus the source evolves instantaneously (Fig. 10 and Table 4). This is obviously not what happens in the real world, but as mentioned earlier is an acceptable approximation of the real problem.

We use a variation of the above model, featuring a Gaussian function along the direction of the 'lever' between trough and hump (Okal *et al.* 2009):

$$z_t = -\eta_t \, e^{-\alpha_t x^2} \, \mathrm{sech}^2(\gamma_t y) \tag{1}$$

$$z_h = \eta_h \, e^{-\alpha_h (x-l)^2} \, \mathrm{sech}^2(\gamma_h y), \tag{2}$$

where l is the length of the lever, η_t and η_h are the depth and height of the trough and hump and α_t, α_h, γ_t and γ_h are coefficients governing the dimensions of each pole along x and y (i.e. directions of sliding and width of the source, respectively), chosen so that the total volume of the hump and the trough are balanced (Okal & Synolakis 2004).

4.4.1 *Bathymetry gradient*

In order to design a legitimate model for an otherwise undocumented underwater landslide like the source of the 1990 tsunami, we first note that its generation requires an adequate slope on which to take place. This rather trivial statement will significantly limit the location of any model of an underwater landslide. Skempton (1953) suggests that submarine landslides tend to occur as a shallow section of ocean floor slips on a slope of 3–6 per cent ($\equiv 12^\circ$–30°), but they can also occur on slopes as low as ∼1 per cent (Prior & Coleman 1984). Prior *et al.* (1982) report slides typically occurring at 4°–10° angles at very shallow depths (2–5 m).

Another trivial but important factor is that landslides are controlled by gravity and therefore the orientation of the lever from trough to hump in Okal & Synolakis' (2004) model should be along the direction of steepest descent of the bathymetry.

Finally, in the case of earthquake-induced landslides, one should place the designed dipole at an appropriate distance from the earthquake source, so that ground acceleration should be sufficient to initialize the slide under an assumed granular scale viscosity characterizing how ready to be destabilized the material may be (e.g. Brunsden & Prior 1984). This is a highly complex problem since the level of ground acceleration at a distance from an earthquake source is a function not only of source size and distance (e.g. Campbell 1997), but also of the possibly heterogeneous local earth structure in between, as well as of any anomalously high stress drop in the seismic source. A classical case in this respect is the rupture by an underwater landslide of telegraphic cables in the Mozambique channel during the Rukwa earthquake of 1910 December 13, as far as 900 km away (Ambraseys 1991).

In this context and following Okal *et al.* (2014), we consider the bathymetry gradient of the southern Caspian Sea. We map on Fig. 11 the modulus of the gradient of the bathymetry, which represents the slope of the ocean floor. It is readily seen that the margins of the southwestern Caspian (close to the 1990 Rudbar earthquake depicted by the red star) feature slopes reaching 8–9 per cent, appropriate for the generation of submarine landslides. In the computation of the bathymetry gradient, we also keep track of its azimuth, which represents the direction of steepest descent on the ocean floor, which we will use to orient the lever of the dipole in our models.

4.4.2 *Different scenarios*

Since the upper sedimentary layers of the Caspian Sea are poorly studied (Levchenko *et al.* 2008), there is not much morphological evidence to pinpoint accurate locations of the past slumps. In the southwestern Caspian Sea, heavy mineral data identify different sediment sources for both Productive series sandstones and modern river sands (Morton *et al.* 2003) and it is believed that the south Caspian sediments are most likely originated from the Alborz mountain range (Morton *et al.* 2003). On the other hand, more data are available for the western coasts of the Caspian Sea where slide-related folded overthrust covers with eastward slopes have been revealed in the Derbent Basin (e.g. Levchenko *et al.* 2008; Putans *et al.* 2010) as possible slump sources.

Based on the slope distribution maps, we designed several possible scenarios with the parameters of the slides in eqs (1) and (2) selected largely in an *ad hoc* fashion. Our purpose here is to document that the main robust characteristic of the results of our survey, namely the distribution of run-up peaked along a ∼30 km stretch of coastline, can be matched by one of these landslide models, featuring legitimate parameters. We emphasize that obviously, the proposed model may not be unique.

Among the many models simulated, we present here six scenarios (A–F), located at the sites featuring the steepest slopes (Fig. 11). In each case, the slide parameters were taken as $\eta_t = 5$ m, $\alpha_t = 0.10\,\mathrm{km}^{-2}$, $\gamma_t = 0.70\,\mathrm{km}^{-1}$, $\eta_h = 3$ m, $\alpha_h = 0.06\,\mathrm{km}^{-2}$, $\gamma_h = 0.54\,\mathrm{km}^{-1}$. The parameters α and γ are chosen to give the slides scaled dimensions comparable to those used in our previous successful models for Papua New Guinea and Amorgos landslides (Synolakis *et al.* 2002; Okal *et al.* 2009). The reason for $\eta_h < \eta_t$ is that submarine slides tend to flatten and disperse over their path (e.g. Okal & Synolakis 2004). The scenarios A–F differ in their position, orientation and length of lever (Table 4). In all cases, the

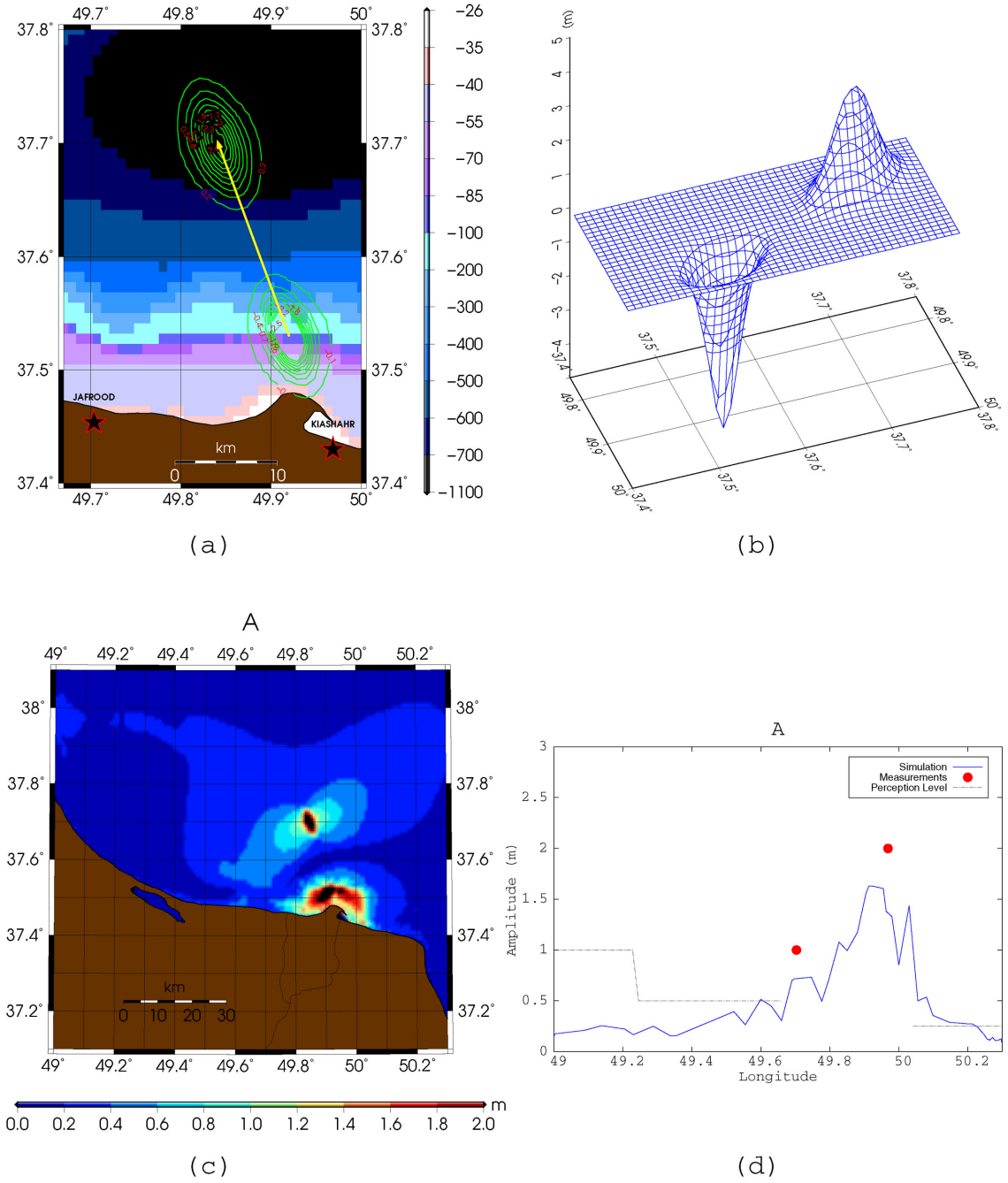

Figure 10. (a) Map view of the successful model (A) with the slump originating at 37.53°N 49.92°E, moving 20 km at the azimuth of 340°. The contour labels are in metres; (b) Schematic of the hump and trough in model A which is created using eqs (1) and (2); (c) The positive maximum amplitude distribution caused by model A; and (d) Distribution of maximum amplitudes along the coastline (blue curve). The red dots are measurements from the survey and the dashed lines are the perception level at the coastline.

Table 4. Slump attributes for models A–F.

Model	Starting latitude (°N)	Starting longitude (°N)	Slide azimuth (°)	Lever length (km)
A	37.53	49.92	340	20
B	37.59	49.51	65	20
C	37.54	49.65	0	20
D	37.47	50.10	30	20
E	37.50	50.03	28	7
F	37.40	50.25	340	20

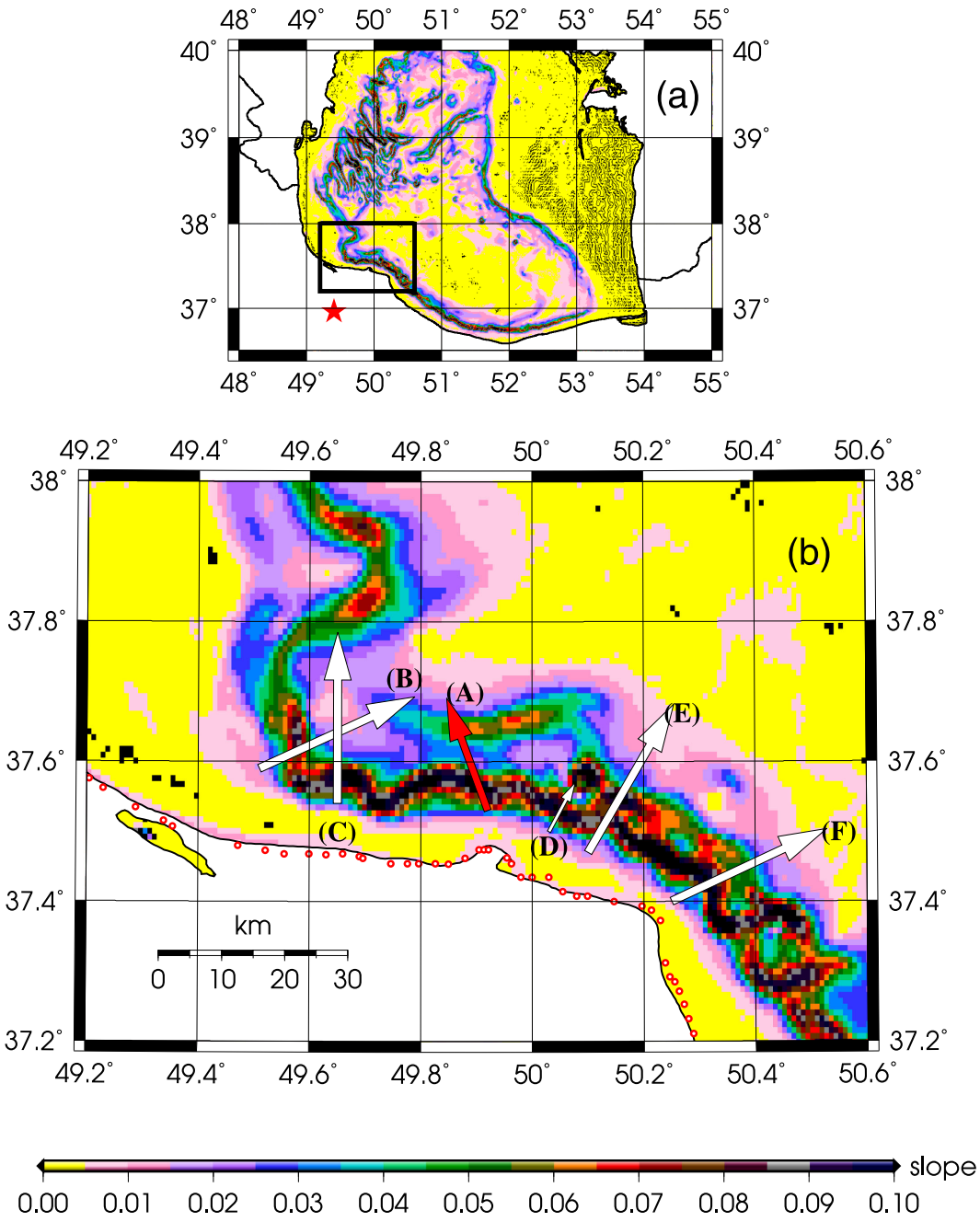

Figure 11. (a) Gradient modulus field of the southern Caspian bathymetry obtained using the GEBCO data set. The black box delineates the area detailed in (b). The red star represents the epicentre of the Rudbar earthquake. (b) Detailed map of six possible slump scenarios as sources of the 1990 tsunami. The red arrow (A) denotes the successful case, shown in more detail in Fig. 10. Red circles are positions of virtual gauges.

parameters γ and α combined with a water depth of ~200 m lead to a dimensionless parameter kh on the order of 0.1 which satisfies the shallow water approximation.

The corresponding slump volume, ~0.1 km^3, remains much smaller than proposed for the 1946 Aleutian (~200 km^3), 1956 Amorgos (~5 km^3) and 1998 Papua New Guinea (~4 km^3) tsunamis (Synolakis *et al.* 2002; Okal *et al.* 2003, 2009). This simply illustrates the fact that the run-ups measured in this study (at most 2 m) were considerably smaller than the 15-m-flow depths surveyed in Papua New Guinea and the 20-m and 42-m run-ups documented in Amorgos and at Unimak Island, respectively.

The simulations were performed using time-steps $\delta t = 4$ s (to satisfy the CFL stability condition) for a 6-hr time window. Time-series were calculated at 128 virtual gauges with particular emphasis on the vicinity of the tsunami reports at Kiashahr (Fig. 11). The computed time-series at Kiashahr and Jafrood from these models are shown in Figs 12(a) and (b).

On Fig. 13, the two red dots represent the run-ups reported at Kiashahr and Jafrood and the stepped dashed lines the maximum acceptable wave heights, estimated from the failure of our witnesses to report any inundation (see discussion in Section 2.1). We emphasize that these figures should be interpreted in terms of

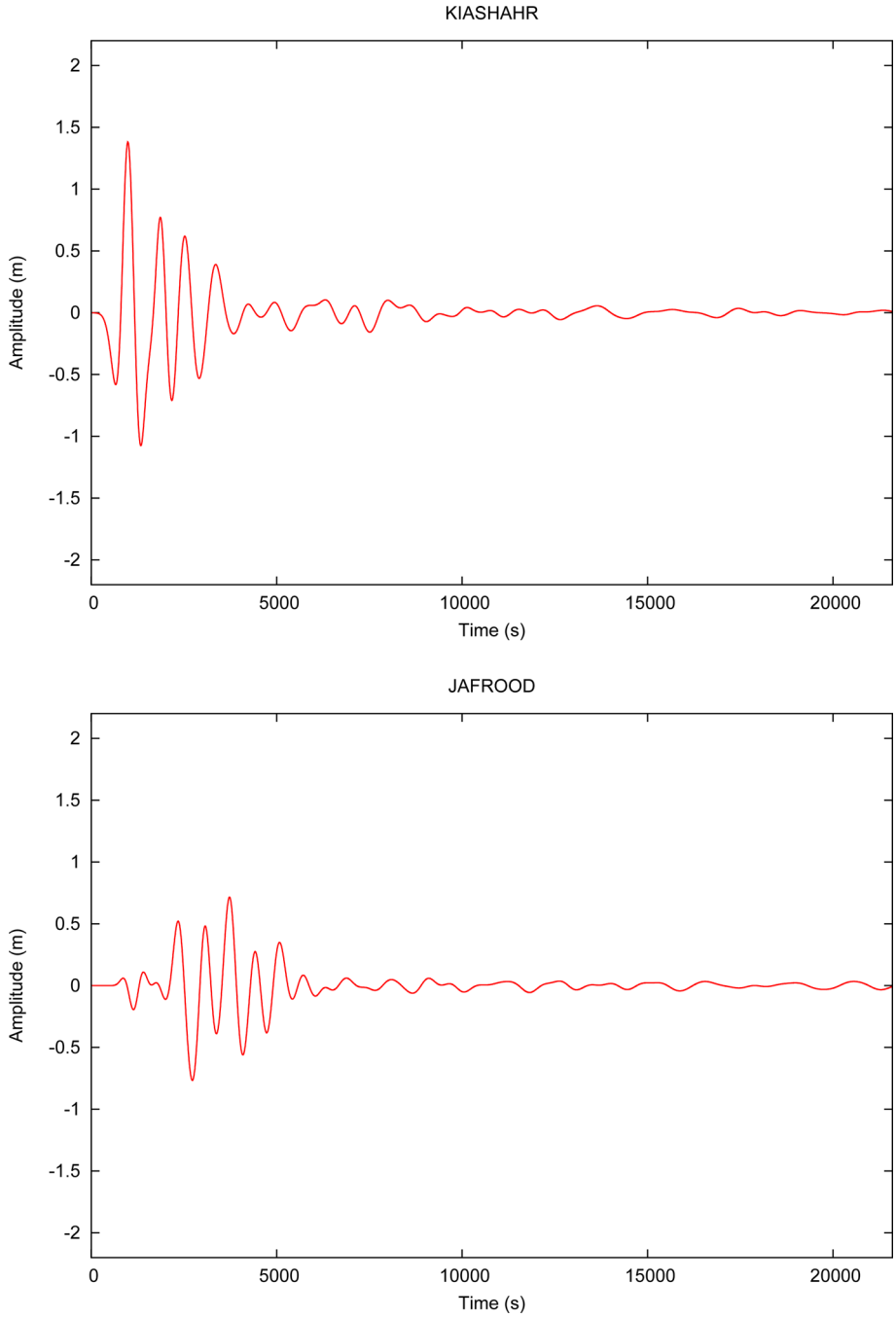

Figure 12. Computed time-series at the two sites with definitive tsunami reports during the 1990 event: (a) Kiashahr and (b) Jafrood. Time 'zero', the beginning of the simulation, corresponds to the onset of the dipole.

relative rather than absolute amplitudes modelled along the coastal profile, since (i) the amplitudes η_l and η_h were selected in an *ad hoc* fashion and (ii) our calculations do not involve the propagation of the waves on initially dry land.

As can be seen in Fig. 10, we regard model (A) as acceptable. Indeed, it gives a good approximation of run-up values at both Jafrood and Kiashahr (only ∼15 per cent less than the reported value) with Kiashahr being very close to the maximum computed run-up. More importantly, wave heights predicted by model (A) remain below the dashed lines of maximum acceptable amplitudes at other locations on the coast. In this respect, Scenario (A) successfully reproduces the concentration of inundation between Kiashahr and Jafrood. Finally, as shown in Fig. 14, the (A) scenario remains reasonably stable while slightly varying the displacement and azimuth of the submarine landslide.

By contrast, models (B) and (C) predict larger amplitudes to the west of Jafrood (which should then have been observed). Models (D) and (E) fail to produce an observable run-up at Jafrood, and model (F) also fails to explain the tsunami at Jafrood and displaces the flooding east of Kiashahr into a zone of minimal acceptable run-up, as characterized by the dashed line on Figs 10 and 13. That leaves (A) as the most successful, and hence most probable, model for the generation of the 1990 tsunami.

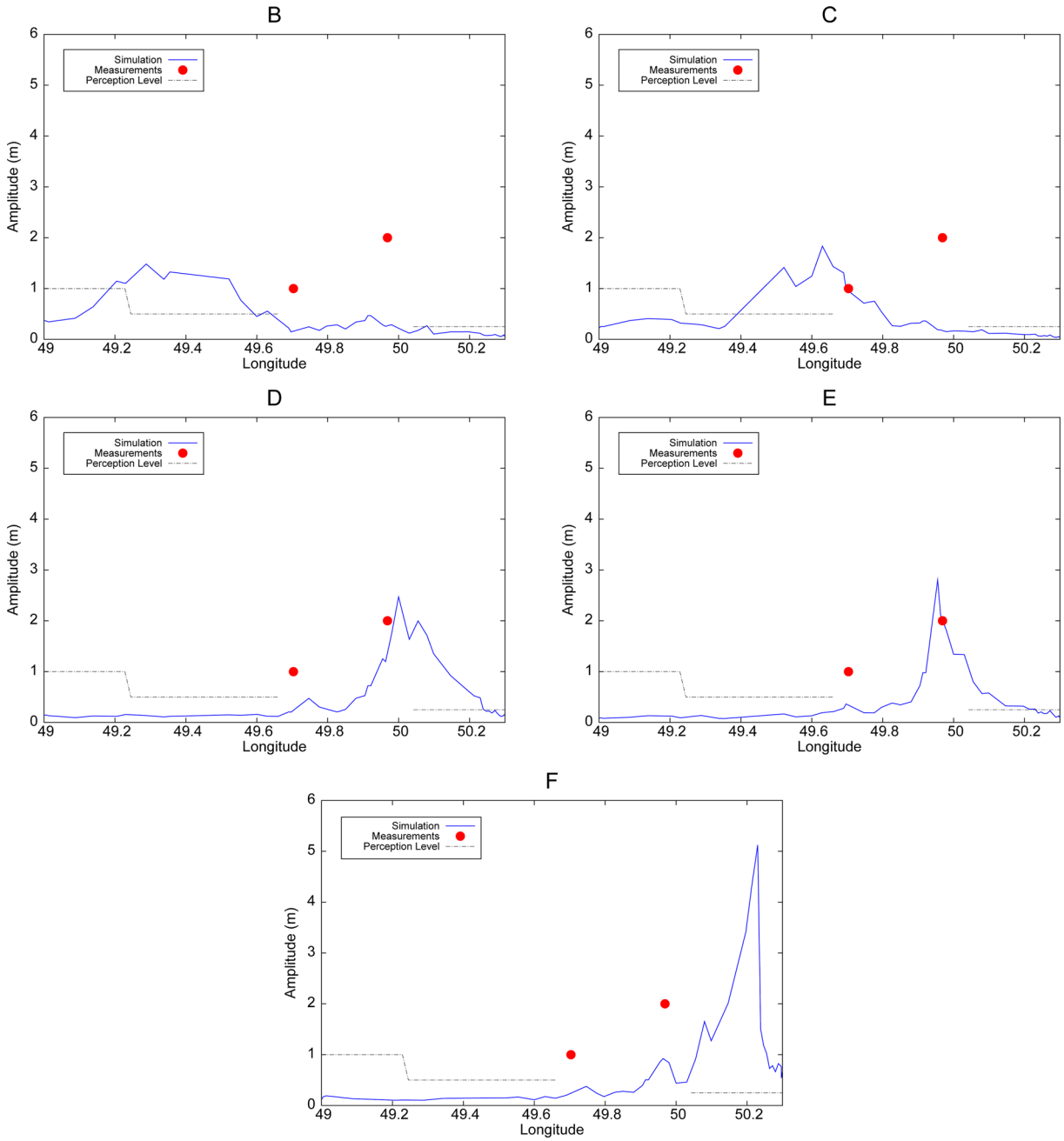

Figure 13. Distribution of maximum amplitudes along the coastline for models B–F.

The dipolar nature of the incoming waves is also clearly seen in Fig. 12(a). In some of the models including the preferred one (A), the initial arrivals at Kiashahr are leading depressions; this is due to the fact that Kiashahr is much closer to the trough (∼60 km) than to the hump (∼140 km). However, in Jafrood which is at comparable distances from the trough (∼100 km) and the hump (∼120 km) the first waves are very small since the elevation and depression effects arrive at almost the same time. In fact, the first small arrival in Jafrood for model (A) is an 'elevation', due to the fact that, at comparable distances, the elevation is located in deeper waters and therefore travels faster.

Unfortunately, we were not able to obtain definitive evidence from our witnesses about the polarity of the first arrivals in the 1990 tsunami, but the above analysis may at least explain why the wave arrivals were more dramatically observed at Kiashahr than at Jafrood during the event (see Table 1).

5 DISCUSSION AND CONCLUSIONS

Our field study, which was initially targeted at documenting Rikhter's (1961) report, failed to identify a legitimate scenario for a definitive inundation in 1960. Rather, we were able to document a significant tsunami following the major Rudbar earthquake of 1990 June 20, with run-up reaching 2 m at Kiashahr and most importantly, a concentration of the inundation over a ∼30 km stretch of coastline.

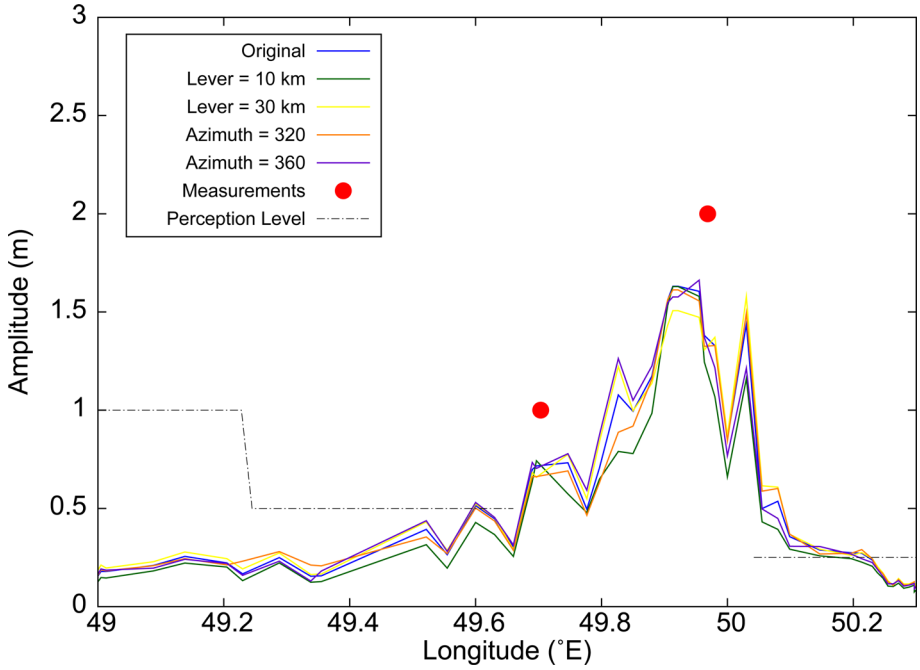

Figure 14. Results of fine-tuning the parameters of the sliding path around the azimuth of 340° and lever length of 20 km (Fig. 10 and Table 4).

These characteristics cannot be modelled using the Rudbar earthquake dislocation as the source of the tsunami since such models grossly underestimate the amplitude of the waves and spread the inundation over a much broader range of coastline including the Gilan province west of 50°E.

By contrast, our model (A) of a landslide, presumably triggered by the earthquake, originating around 37.53°N, 49.92°E, and extending 20 km in a 340° azimuth (red arrow on Fig. 11), manages to match the general profile of the reported tsunami along the coast. In this model, the head of the slide is located 80 km from the epicentre and less than 10 km from the coastline, where the earthquake was felt at MMI VI (Berberian *et al.* 1992), suggesting horizontal accelerations of ∼1 m s^{-2} (0.1 g). This level of intensity is described as a general lower bound for the triggering of landslides (Keefer 1984), with several documented occurrences at even lower intensities. In this context, it appears legitimate to invoke the triggering of the landslide modelled as (A) by the 1990 earthquake, especially given its location immediately offshore of the delta of the Sefidrood River, expected to contribute significant sediment discharge in the area. In this context, we note that aerial landslides were documented as a result of the 1990 event at Jamalabad and Baklor, ∼30 km from the epicentre (Berberian *et al.* 1992).

Finally, the delay (∼2 hr) reported at Kiashahr between the shaking during the earthquake and the onset of the tsunami could be related to the non-linearity of the triggering process, probably involving an evolution of fluid pore pressure inside the rock. We recall that a delay of 13 min took place before the triggering of the landslide responsible for the 1998 Papua New Guinea tsunami, which occurred at a location generally estimated to be closer to the fault rupture than in this case (Synolakis *et al.* 2002).

At this point, model (A) remains somewhat speculative in the absence of an independent verification of an appropriate footprint on the ocean floor, as in the case of the 1998 Papua New Guinea event (Sweet & Silver 2003) and possibly of the 1946 Aleutian event (Miller *et al.* 2014). In the present case and unfortunately, there are no accessible high resolution maps from the sea bed at the vicinity of the location of scenario (A) to confirm this model and therefore not much could be said about the geometry of the slide. The only notable displaced mass in the southern slopes (Fig. 15) could represent the hump for the (D) scenario in Fig. 11, a model which fails to reproduce high run-up values in Jafrood. Alternatively, it may correspond to a previous episode of slumping.

Similarly, there exists no seismological evidence of the proposed landslide. In the case of the 1998 Papua New Guinea, we were able to identify among reported aftershocks a signal deviating from earthquake scaling laws which we interpreted as the seismic signature of the landslide (Okal 2003). In the present case, however, no reported aftershock occurs inside the Caspian Sea before the reported time of the tsunami, and furthermore, it is probable that the small size of the proposed landslide (0.1 km^3) would not have given rise to a detectable signal, especially given the lack of seismic stations in the immediate vicinity of the epicentre.

In conclusion, our study sheds new light on tsunami hazard on the Iranian coast of the Caspian Sea. The testimony of our witnesses confirms that a tsunami did take place following the 1990 Rudbar earthquake, the largest event recorded in northern Iran in modern times, even though it remained relatively modest and its flooding resulted in no significant damage or casualties. Our failure to explain the tsunami as generated by the elastic dislocation and our success at modelling its concentration along a ∼30 km stretch of coastline using a landslide as its source, suggest that landslides should be regarded as a, if not the, major contributor to tsunami hazard along the Iranian coast of the Caspian Sea. It is in this context that historical accounts describing more severe episodes of flooding (e.g. Gerasimov 1978; Ambraseys & Melville 1982) should be re-investigated.

While landslide tsunami hazard is inherently more difficult to assess on account of the extreme non-linearity of the phenomenon, the risk along the Caspian Sea may be somewhat mitigated by the capricious fluctuations of the sea level, occasionally on very short timescales, which have led to a general awareness of coastal hazards on the part of the population.

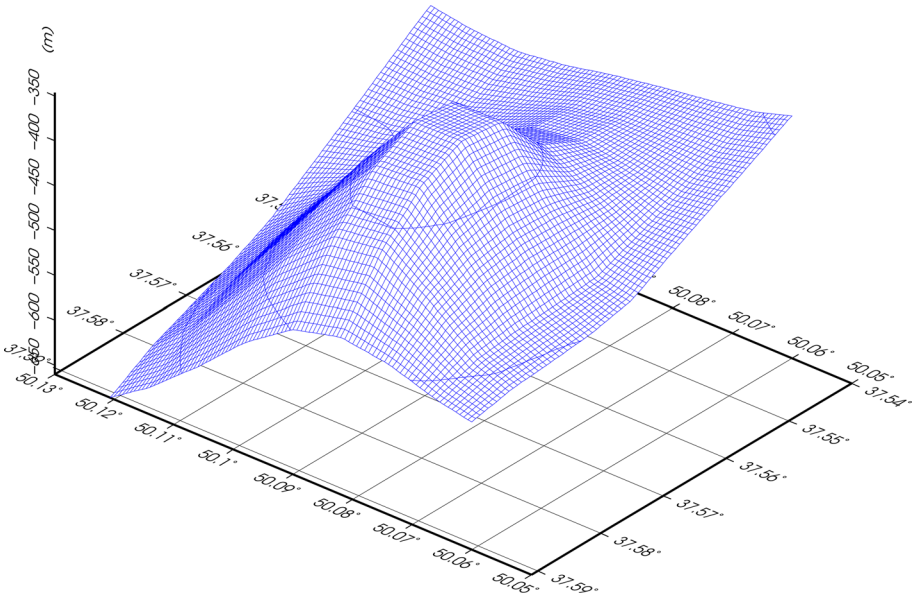

Figure 15. The seemingly displaced mass which is the reason for designing the (D) scenario. The nature of this bathymetry anomaly could not be further studied, due to the non-adequate resolution of the available bathymetry maps.

ACKNOWLEDGEMENTS

The authors wish to thank the Iranian National Institute for Oceanography (INIO) for logistic coordinations and general help during the 2012 fieldwork on the Iranian coastlines of the Caspian Sea. INIO also provided the survey with some of the necessary paperwork in order to perform fieldwork along the coastlines and to explore coastal archives in Noshahr and Anzali ports.

We thank Mathieu Rodriguez and an anonymous reviewer for constructive comments on the initial versions of the paper.

Some of the figures were created using the Generic Mapping Tools (GMT; Wessel & Smith 1991) and Gnuplot (Williams & Kelley 2009) software packages.

REFERENCES

Aghanabati, A., 2004. *Geology of Iran,* Geological Survey of Iran.

Amante, C. & Eakins, B.W., 2009. ETOPO1 1 Arc-Minute Global Relief Model: Procedures, Data Sources and Analysis, US Department of Commerce, National Oceanic and Atmospheric Administration, National Environmental Satellite, Data, and Information Service, National Geophysical Data Center, Marine Geology and Geophysics Division.

Ambraseys, N., 1991. The Rukwa earthquake of 13 December 1910 in East Africa, *Terra Nova,* **3**(2), 202–211.

Ambraseys, N., 1997. The Krasnovodsk (Turkmenistan) earthquake of 8 July 1895, *J. Earthq. Eng.,* **1**(2), 293–317.

Ambraseys, N.N. & Melville, C.P., 1982. *A History of Persian Earthquakes,* Cambridge Univ. Press.

Barberopoulou, A., Qamar, A., Pratt, T.L., Creager, K.C. & Steele, W.P., 2004. Local amplification of seismic waves from the Denali Earthquake and damaging seiches in Lake Union, Seattle, Washington, *Geophys. Res. Lett.,* **31**(3), L03607, doi:10.1029/2003GL018569.

Berberian, M. & Walker, R., 2010. The Rudbār Mw 7.3 earthquake of 1990 June 20; seismotectonics, coseismic and geomorphic displacements, and historic earthquakes of the western High-Alborz, Iran, *Geophys. J. Int.,* **182**(3), 1577–1602.

Berberian, M., Qorashi, M., Jackson, J., Priestley, K. & Wallace, T., 1992. The Rudbar-Tarom earthquake of 20 June 1990 in NW Persia: preliminary field and seismological observations, and its tectonic significance, *Bull. seism. Soc. Am.,* **82**(4), 1726–1755.

Brunsden, D. & Prior, D.B., 1984. *Slope Instability,* John Wiley and Sons.

Campbell, K.W., 1997. Empirical near-source attenuation relationships for horizontal and vertical components of peak ground acceleration, peak ground velocity, and pseudo-absolute acceleration response spectra, *Seismol. Res. Lett.,* **68**(1), 154–179.

Campos, J., Madariaga, R., Nábělek, J., Bukchin, B. & Deschamps, A., 1994. Faulting process of the 1990 June 20 Iran earthquake from broadband records, *Geophys. J. Int.,* **118**(1), 31–46.

Chinnery, M., 1961. The deformation of the ground around surface faults, *Bull. seism. Soc. Am.,* **51**(3), 355–372.

Cisternas, M. *et al.*, 2005. Predecessors of the giant 1960 Chile earthquake, *Nature,* **437**(7057), 404–407.

Dotsenko, S., Kuzin, I., Levin, B. & Solovieva, O., 2001. Tsunamis in the Caspian Sea: numerical modeling of tsunami propagation from the zones of seismic generation, *Oceanology,* **41**(3), 345–350.

Dotsenko, S.F., Kuzin, I.P., Levin, B.V. & Solovieva, O.N., 2002. Tsunamis in the Caspian Sea: historical events, regional seismicity and numerical modeling, in *Proceedings of the International Workshop "Local Tsunami Warning and Mitigation",* Petropavlovsk-Kamchatsky, Russia, pp. 23–31.

EHB Bulletin 2009. International Seismological Centre, Int. Seis. Cent., Thatcham, United Kingdom, http://www.isc.ac.uk.

Fisher, R., Jantsch, M. & Comer, R., 1982. *General Bathymetric Chart of the Oceans (GEBCO)*, Canada Hydrographic Service.

Gao, L. & Wallace, T.C., 1995. The 1990 Rudbar-Tarom Iranian earthquake sequence: evidence for slip partitioning, *J. geophys. Res.: Solid Earth,* **100**(B8), 15 317–15 332.

Geller, R.J., 1976. Scaling relations for earthquake source parameters and magnitudes, *Bull. seism. Soc. Am.,* **66**(5), 1501–1523.

Gerasimov, I., 1978. The past and the future of the Aral and the Caspian Seas, *The Environmental History of the Near and Middle East,* pp. 335–349, ed. Brice, W.C., Academic Press.

Gutenberg, B., 1939. Tsunamis and earthquakes, *Bull. seism. Soc. Am.,* **29**(4), 517–526.

Hammack, J.L., 1973. A note on tsunamis: their generation and propagation in an ocean of uniform depth, *J. Fluid Mech.,* **60**(4), 769–799.

Hedin, S., 1892. Der Demavand nach eigener Beobachtung, *Verhandlung der Ges. fur Erdkd. zu Berlin,* **19,** 304.

Heinrich, P., 1992. Nonlinear water waves generated by submarine and aerial landslides, *J. Waterway, Port, Coast., Ocean Eng.,* **118**(3), 249–266.

Hoffmann, G., Al-Yahyai, S., Naeem, G., Kociok, M. & Grützner, C., 2014. An Indian Ocean tsunami triggered remotely by an onshore earthquake in Balochistan, Pakistan, *Geology,* **42**(10), 883–886.

Imamura, A. & Kennedy, D., 1937. *Theoretical and Applied Seismology,* Maruzen Company.

Ishihara, K., Haeri, M., Minofar, A.A., Towhata, I. & Tsujino, S., 1992. Geotechnical aspects of the June 20, 1990 Manjil earthquake in Iran, *Soils Found.,* **32**(3), 61–78.

Jackson, J., Priestley, K., Allen, M. & Berberian, M., 2002. Active tectonics of the South Caspian basin, *Geophys. J. Int.,* **148**(2), 214–245.

Kagan, Y., 1991. 3-D rotation of double-couple earthquake sources, *Geophys. J. Int.,* **106**(3), 709–716.

Keefer, D.K., 1984. Landslides caused by earthquakes, *Geol. Soc. Am. Bull.,* **95**(4), 406–421.

Kondorskaya, N., Shebalin, N.V., Khrometskaya, Y. & Gvishiani, A., 1982. *New Catalog of Strong Earthquakes in the USSR from Ancient Times Through 1977,* World Data Center A for Solid Earth Geophysics.

Kvale, A., 1955. Seismic Seiches in Norway and England during the Assam earthquake of August 15, 1950, *Bull. seism. Soc. Am.,* **45**(2), 93–113.

Levchenko, O., Verzhbitskii, V. & Lobkovskii, L., 2008. Submarine landslide structures in neopleistocene deposits on the western slope of the Derbent basin of the Caspian Sea, *Oceanology,* **48**(6), 864–871.

Locat, J. & Lee, H.J., 2002. Submarine landslides: advances and challenges, *Can. Geotech. J.,* **39**(1), 193–212.

Ma, G., Kirby, J.T. & Shi, F., 2013. Numerical simulation of tsunami waves generated by deformable submarine landslides, *Ocean Modell.,* **69,** 146–165.

Mansinha, L. & Smylie, D., 1971. The displacement fields of inclined faults, *Bull. seism. Soc. Am.,* **61**(5), 1433–1440.

McGarr, A. & Vorhis, R.C., 1968. Seismic seiches from the March 1964 Alaska earthquake, *US Geol. Surv. Profess. Paper,* **544,** 1–23.

Miller, J.J., von Huene, R. & Ryan, H., 2014. The 1946 Unimak tsunami earthquake area: revised tectonic structure in reprocessed seismic images and a suspect near field tsunami source, U.S. Geological Survey Open-File Report (2014–1024), 1–22.

Mirzaei, N., Gao, M. & Chen, Y.-t., 1999. Delineation of potential seismic sources for seismic zoning of Iran, *J. Seismol.,* **3**(1), 17–30.

Montessus de Ballore, F.C., 1907. La science Séismologique: les tremblements de terre, pp. 220–221.

Morton, A., Allen, M., Simmons, M., Spathopoulos, F., Still, J., Hinds, D., Ismail-Zadeh, A. & Kroonenberg, S., 2003. Provenance patterns in a neotectonic basin: Pliocene and Quaternary sediment supply to the South Caspian, *Basin Res.,* **15**(3), 321–337.

Okada, Y., 1985. Surface deformation due to shear and tensile faults in a half-space, *Bull. seism. Soc. Am.,* **75**(4), 1135–1154.

Okal, E.A., 2003. T waves from the 1998 Papua New Guinea earthquake and its aftershocks: timing the tsunamigenic slump, *Pure appl. Geophys.,* **160,** 1843–1863.

Okal, E.A. & Synolakis, C.E., 2004. Source discriminants for near-field tsunamis, *Geophys. J. Int.,* **158**(3), 899–912.

Okal, E.A., Plafker, G., Synolakis, C.E. & Borrero, J.C., 2003. Near-field survey of the 1946 Aleutian tsunami on Unimak and Sanak Islands, *Bull. seism. Soc. Am.,* **93**(3), 1226–1234.

Okal, E.A., Synolakis, C.E., Uslu, B., Kalligeris, N. & Voukouvalas, E., 2009. The 1956 earthquake and tsunami in Amorgos, Greece, *Geophys. J. Int.,* **178**(3), 1533–1554.

Okal, E.A., Visser, J.N. & de Beer, C.H., 2014. The Dwarskersbos, South Africa local tsunami of August 27, 1969: field survey and simulation as a meteorological event, *Nat. Hazards,* **74,** 1–18.

Ozyavas, A. & Khan, S.D., 2012. The driving forces behind the Caspian Sea mean water level oscillations, *Environ. Earth Sci.,* **65**(6), 1821–1830.

Polyakov, A. *et al.*, 2010. Estimation of parameters of the flows forming sediment waves on the western slope of the middle Caspian Sea, *Doklady Earth Sci.,* **431**(1), 376–379.

Priestley, K., Baker, C. & Jackson, J., 1994. Implications of earthquake focal mechanism data for the active tectonics of the South Caspian basin and surrounding regions, *Geophys. J. Int.,* **118**(1), 111–141.

Prior, D.B. & Coleman, J.M., 1984. *Submarine Slope Instability,* Louisiana State University Coastal Studies Institute.

Prior, D.B., Bornhold, B.D., Coleman, J.M. & Bryant, W.R., 1982. Morphology of a submarine slide, Kitimat Arm, British Columbia, *Geology,* **10**(11), 588–592.

Putans, V.A. *et al.*, 2010. Sediment waves and other forms as evidence of geohazards in Caspian Sea, *Int. J. Offshore Polar Eng.,* **20**(4), 241.

Reymond, D., Okal, E., Hébert, H. & Bourdet, M., 2012. Rapid forecast of tsunami wave heights from a database of pre-computed simulations, and application during the 2011 Tohoku tsunami in French Polynesia, *Geophys. Res. Lett.,* **39**(11), L11603, doi:10.1029/2012GL051640.

Rikhter, V., 1961. Vertical movements of the earth crust and the fluctuations in the level of the Caspian Sea, *Soviet Geogr.,* **2**(7), 59–64.

Rychagov, G., 1997. Holocene oscillations of the Caspian Sea, and forecasts based on palaeogeographical reconstructions, *Quater. Int.,* **41,** 167–172.

Scholz, C.H., 1982. Scaling laws for large earthquakes: consequences for physical models, *Bull. seism. Soc. Am.,* **72**(1), 1–14.

Skempton, A., 1953. Soil mechanics in relation to geology, *Proc. Yorkshire Geol. Soc.,* **29**(1), 33–62.

Soltanpour, M. & Rastgoftar, E., 2011. Study of tsunami attacks on neighboring countries of Caspian Sea caused by a probable submarine landslide, *J. Coastal Res.,* **SI64,** 1195–1199.

Sweet, S. & Silver, E., 2003. Tectonics and slumping in the source region of the 1998 Papua New Guinea tsunami from seismic reflection images, *Pure appl. Geophys.,* **160,** 1945–1968.

Synolakis, C.E., Bardet, J.-P., Borrero, J.C., Davies, H.L., Okal, E.A., Silver, E.A., Sweet, S. & Tappin, D.R., 2002. The slump origin of the 1998 Papua New Guinea tsunami, *Proc. R. Soc. Lond., A: Math., Phys. Eng. Sci.,* **458,** 763–789.

Synolakis, C.E., Bernard, E., Titov, V., Kânoğlu, U. & González, F., 2008. Validation and verification of tsunami numerical models, *Pure appl. Geophys.,* **165**(11–12), 2197–2228.

Tatar, M. & Hatzfeld, D., 2009. Microseismic evidence of slip partitioning for the Rudbar-Tarom earthquake (M_s 7.7) of 1990 June 20 in NW Iran, *Geophys. J. Int.,* **176**(2), 529–541.

Titov, V.V. & González, F.I., 1997. Implementation and Testing of the Method of Splitting Tsunami (MOST) Model, US Department of Commerce, National Oceanic and Atmospheric Administration, Environmental Research Laboratories, Pacific Marine Environmental Laboratory.

Titov, V.V. & Synolakis, C.E., 1995. Modeling of breaking and nonbreaking long-wave evolution and runup using VTCS-2, *J.Waterway, Port, Coast., Ocean Eng.,* **121**(6), 308–316.

Titov, V.V. & Synolakis, C.E., 1998. Numerical modeling of tidal wave run-up, *J. Waterway, Port, Coast., Ocean Eng.,* **124**(4), 157–171.

Verbeek, R., 1900. Kort verslag over de aard- en zeebevingen op Ceram, den 30 September, 1899, *Natuurkund. Tijdschr. voor Ned.-Indie,* **60,** 218.

Vernant, P. *et al.*, 2004. Deciphering oblique shortening of central Alborz in Iran using geodetic data, *Earth planet. Sci. Lett.,* **223**(1), 177–185.

Verzhbitskii, V., Levchenko, O. & Lobkovskii, L., 2009a. On gravitational instability of Quaternary sediments on the western slope of the Derbent basin (Caspian Sea), *Doklady Earth Sci.,* **428**(1), 1179–1182.

Verzhbitskii, V. *et al.*, 2009b. Slump structures in Quaternary slope sediments of the northern Derbent Basin (Caspian Sea), *Oceanology,* **49**(3), 396–404.

Virieux, J., Deschamps, A., Perrot, J. & Campos, J., 1994. Source mechanisms and near-source wave propagation from broadband seismograms, *Ann. Geophys.,* **37**(6), 1565–1590.

Weiss, R., Krastel, S., Anasetti, A. & Wünnemann, K., 2013. Constraining the characteristics of tsunami waves from deformable submarine slides, *Geophys. J. Int.,* **194**(1), 316–321.

Wessel, P. & Smith, W.H., 1991. Free software helps map and display data, *EOS, Trans. Am. geophys. Un.,* **72**(41), 441–446.

Williams, T. & Kelley, C., 2009. Gnuplot 4.2: An interactive plotting program, http://gnuplot.sourceforge.net/.

Yanenko, N.N., 1971. *The Method of Fractional Steps,* Springer.

Zaitsev, A.I., Kurkin, A.A. & Pelinovsky, E.N., 2004. Historical tsunamis of the Caspian Sea and their modeling, *Izv. AIN RF, Series: Appl. Math. Mech.,* **9,** 121–134.

APPENDIX: THE CASE OF THE 1960(?) EVENT

The report of this event by Rikhter (1961) is mentioned by Ambraseys & Melville (1982, p. 107). However, we discount Rikhter's (1961) interpretation as an event triggered by a local earthquake based on the following remarks:

First, we could not identify a suitable Iranian seismic event in any available catalogue (e.g. Ambraseys & Melville 1982; EHB Bulletin 2009). The only potential candidate would seem to be the $M_S = 6.0$ earthquake on 1960 April 24 at 12:14 UTC, but this event took place in Zagros in southern Iran (more than 1400 km away) and its radius of perception was only 100 km (Ambraseys & Melville 1982). Second, a delay of two days would clearly require generation by an auxiliary phenomenon. A smaller event with no reported magnitude also took place on 1960 April 24 at 06:00 GMT, but its location is well constrained near Erzican, Turkey on the North Anatolian Fault. Finally, the reported periods of the oscillation (upwards of 2 hr) would require, even in shallow waters, wavelengths and hence faulting dimensions incommensurate with those of the Zagros earthquake or of another event which would have escaped worldwide detection.

Nevertheless, we were intrigued by Rikhter's (1961) report which suggested that living witnesses might still be interviewed to cast some light on its occurrence. This initially motivated our field survey which eventually revealed the 1990 Rudbar tsunami.

During the field survey, we obtained four reports dating 40–50 yr which could, at least conceivably, be associated with the 1960 event described by Rikhter, as discussed below. However, these reports were very scattered and vague (see the quality column in Table 1). Interviews at Shirood and Limir (numbers 9 and 27 in Table 1) pointed to seismic events in the 1960s or 1970s possibly correlated with wave activity, but these reports were dubious and at any rate not quantitative. However, we obtained a more credible report at Siahchal (number 22 in Table 1) in which an elderly witness vividly remembered an earthquake accompanied by sea water surges.

Siahchal is a farming fishing village in the Gilan province on the east of Talesh (a.k.a. Hashtpar). There are numerous citrus orchards on the farms near the coastal area as well as many rice farmlands on the coastal stretch. Musa Bordbar (born in 1931), a farmer (who was formerly a fisherman) in Siahchal, remembers an earthquake in the late 1950s or early 1960s.

According to Musa, this earthquake had happened in the Spring (or perhaps Summer), before noon time. He also recalled hearing of three women and one man who had lost their lives—not in Siahchal—as a result of the event, which confirms the occurrence of a serious earthquake. The witness vividly remembered the ground (somewhat close to the sea) opening and closing, spurting water onto the ground, a classical episode of liquefaction. At the time of the event, he had been on his way to spread fishing nets, when he saw the sea inundating the land up to 60 m, creating run-ups close to 1 m. He told us that the wave height increased as it approached the land. He also remembered 5 waves and that the waves were moving due South.

Musa's recollection was the only rigorous observation (grade *a* in the quality scale of Table 1). A search of available catalogues (e.g. Kondorskaya *et al.* 1982; EHB Bulletin 2009) may reconcile it with the event of 1961 June 9, 09:36 GMT northeast of Baku (400 km away) which would match both the season and time of the day. ($M_S = 6.0$; EHB Bulletin (2009)). However, this 1961 earthquake is not reported to have inflicted significant damage in Baku (∼70 km from the epicentre) which raises doubts that it would have resulted in destruction and fatalities in Iran at ∼6 times the distance. Therefore, its correlation with our witness's account is highly doubtful. It is also highly improbable that this earthquake occurring in June 1961 could have been included in Rikhter's (1961) publication, which has a timeline of March–April 1961, as it would require considerable delays in publication. In conclusion, Musa's report, although of a precise, quantitative and apparently persuasive character, cannot be reconciled with a documented local earthquake.

Another possible interpretation of Rikhter's (1961) report could be seiching induced in the Caspian Sea by a large distant earthquake. Teleseismic seiching was reported following the mega earthquakes of Assam, 1950 (in fjords of Norway, Kvale 1955) and Alaska, 1964 (principally in estuaries in Texas McGarr & Vorhis 1968), and at shorter distances in Lake Union, Seattle, following the 2003 Denali, Alaska earthquake (Barberopoulou *et al.* 2004), following the transit of conventional surface waves. In the present case, the only candidate, which would involve a 1-month error in the date of the event, would be the Chilean earthquake of 1960 May 22. However, we dismiss this possibility since the periods of self-oscillation of the Caspian Sea (or at least its southern basin) would be on the order of several thousand seconds; this might agree with the description by Rikhter (1961), but would be outside the domain of propagating surface waves; in addition, seiching was reported only regionally following the 1960 Chilean event. Finally, the timing of the event would also be impossible to reconcile with the witness account of Siahchal since surface waves from the Chilean 1960 earthquake would arrive in Iran around midnight local time.

At this stage, we speculate that the most probable origin of the phenomenon described by Rikhter (1961) would have to be meteorological; however, we re-emphasize that this would not agree with the lone testimony obtained at Siahchal, which associated the flooding with a felt earthquake. The two events, if real, have to be different.

In conclusion, this survey, originally meant to document the observation reported by Rikhter (1961), resulted in only one witness report with a potentially suitable date. However, we could not establish an acceptable correlation between that witness's description, Rikhter's speculative report, and available scientific catalogues of seismicity. The lone witness report (suffering from imprecision concerning its date) remains ambiguous and therefore cannot be studied further.